

Stratified flow past a sphere

By Q. LIN¹, W. R. LINDBERG², D. L. BOYER¹ AND
H. J. S. FERNANDO¹

¹ Department of Mechanical and Aerospace Engineering, Arizona State University,
Tempe, AZ 85287-6106, USA

² Department of Mechanical Engineering, University of Wyoming, Laramie,
Wyoming 82071-3295, USA

(Received 3 November 1990 and in revised form 20 December 1991)

The flow of a linearly stratified fluid past a sphere is considered experimentally in the Froude number Fi , Reynolds number Re , ranges $0.005 \leq Fi \leq 20$ and $5 \leq Re \leq 10000$. Flow visualization techniques and density measurements are used to describe the rich range of characteristic flow phenomena observed. These different flow patterns are mapped on a detailed Fi against Re flow regime diagram. In most instances the flow patterns were found to be very different from those observed in homogeneous fluids. Vortex shedding characteristics, for example, were found to be dramatically affected by the presence of stratification. Where possible, the results are compared with available analytical and numerical models.

1. Introduction

The study of wakes formed by the steady motion of blunt three-dimensional obstacles through both homogeneous and stratified fluids has been of long-standing interest to the fluid dynamics community. The most fundamental geometry in this regard is that of the sphere and the most basic fluid is that for which the medium is homogeneous and incompressible. It is well known that the flow character for this configuration, assuming that bounding surfaces are far from the sphere, depends on a single parameter, the Reynolds number $Re = UD/\nu$, where U is the free-stream speed, D the sphere diameter and ν the kinematic viscosity. Surveys of the literature on this problem are contained, for example, in the papers by Torobin & Gauvin (1959, 1960) and Pao & Kao (1977).

For $Re \lesssim 1$ the classical Stokes and Oseen approximations can be applied with the flow being fully attached to the sphere. The structure of the wake at moderate Reynolds numbers (i.e. $1 \lesssim Re \lesssim 2000$) has been discussed by Rosenhead (1953), Taneda (1956), Magarvey & MacLachy (1965), Achenbach (1974), Nakamura (1976), Pao & Kao (1977), Kim & Durbin (1988), among others. For $Re \gtrsim 25$, the flow begins to separate forming a bubble region on the downstream side of the sphere; see Nakamura (1976). Taneda (1956) has discussed this attached bubble region flow regime both theoretically and experimentally; his experiments were in the range $9 \lesssim Re \lesssim 133$. Taneda's study shows that the size and extent of the bubble region increases with Re , with unsteady wake flows first becoming apparent at $Re \gtrsim 130$. Nakamura suggests that steady flows can be observed to $Re \approx 190$. For $Re \gtrsim 400$ the unsteady attached bubble begins to shed periodically from the sphere and advect downstream. Some suggestions on the nature of the shed vortices have been made by Achenbach (1974) and Pao & Kao (1977), however, the actual structure is still

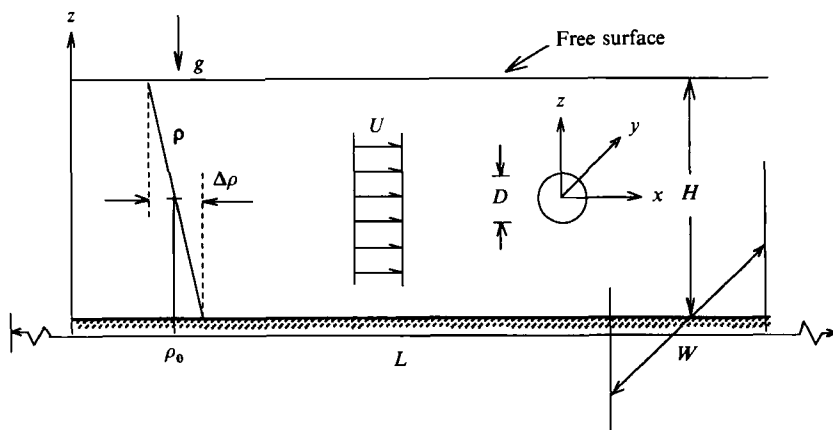


FIGURE 1. Physical system.

unclear. The wake becomes turbulent when the Reynolds number is larger than about 2000.

The case of flow past a sphere for fluid systems which are continuously (linearly) stratified is the focus of the present investigations. The study of such flows is motivated by potential applications to geophysical systems such as the flow past topographic features of limited horizontal extent in the atmosphere or oceans (i.e. stratification is important but background rotation is not), self-propelled bodies moving through the oceanic thermocline and currents impinging on offshore structures and moorings.

The physical system considered herein is sketched schematically in figure 1. A liquid of mean density ρ_0 and constant buoyancy frequency $N = [(g/\rho_0)(\partial\rho/\partial z)]^{1/2}$ is in uniform rectilinear motion U past a sphere of diameter D , g is the acceleration of gravity and ρ the density. The flow takes place in a tank of length L , width W and the fluid has a depth H . The bottom, ends and sides of the tank are plane solid surfaces, while the upper boundary is free. In the experiments, the stratification is established using salt water, as described below, and the fluid motion is realized by towing the sphere through a fluid otherwise at rest with respect to the tank. We will refer to the rectangular Cartesian coordinate system (x, y, z) relative to an observer fixed to the sphere.

From dimensional analysis the characteristics of the flow should depend on the following parameters:

$$Fi = \frac{U}{ND}, \quad \text{internal Froude number,}$$

$$Re = \frac{UD}{\nu}, \quad \text{Reynolds number,}$$

$$Sc = \frac{\nu}{\kappa}, \quad \text{Schmidt number and}$$

$$\frac{D}{W}, \frac{D}{L}, \frac{D}{H}, \quad \text{geometrical parameters.}$$

It is assumed that the times over which the experiments are conducted are substantially less than the timescales for salt diffusion and that the density gradients

in all regions of the flow are not too large; the Schmidt number is thus unimportant. It is further assumed that $W, L, H \gg D$ so that geometrical effects may be neglected. The problem is thus reduced to a two-parameter one; i.e. Fi and Re . The initial objective of the study will be to describe the rich variety of flows that are observed as these parameters are varied over the practical range of the experimental systems employed; i.e. $0.005 \leq Fi \leq 20$ and $5 \leq Re \leq 10000$. This portion of the work follows closely the similar investigation by Boyer *et al.* (1989) for a horizontal right circular cylinder.

The second objective is to quantify the observed flow fields, to apply scaling analyses and to compare with available theories, so as to understand more fully the physical processes involved; these studies will include such observable quantities as dividing streamline heights, lee-wave parameters and characteristics of shed vortices. Before discussing the present experiments, let us consider some other recent studies of stratified flow past a sphere and other three-dimensional obstacles.

The ability of a stratified fluid to propagate internal wave motions is of fundamental importance in the flow behaviour in a stratified environment. One could compare the motion of a sphere moving horizontally through a stratified fluid with a three-dimensional internal-wave disturbance which propagates with a phase speed the same as the sphere's velocity. At low Fi , the wavelength of the resulting waves is quite small compared to the size of the sphere. The vertical motion adjacent to the sphere would then also be small. At higher Fi , the corresponding wave field (and fluid kinetic energy) would be sufficiently energetic for significant vertical motions to exist. For disturbance velocities with wavelengths comparable to the diameter of the sphere, the wave field intensifies, creating velocity and pressure distributions adjacent to the body which are quite different from those observed at lower speeds. The potential for the velocity and pressure fields to significantly alter the boundary-layer flow, separation behaviour and wake structure thus exists.

The limiting cases of $Fi \gg 1$ and $Fi \ll 1$ are useful considerations in addressing the general problem. In the limit of very small Froude numbers, the fluid is constrained to flow around the object, rather than over or under it. In this quasi two-dimensional case, the flow at any given depth should resemble the flow around a vertical two-dimensional cylinder whose cross-section is the same as the object's cross-section at that elevation. The low $Re-Fi$ theory of Drazin (1961), which was extended by Brighton (1978), is based on a perturbation of this two-dimensional behaviour, where any vertical displacements in the fluid are seen to be of the order of Fi^2 . For very large Froude numbers, on the other hand, the flow would be expected to resemble the unstratified flow behaviour discussed above. In fact, in one of the more descriptive discussions of the wake behaviour of a homogeneous flow past a sphere, Pao & Kao (1977) used a slightly stratified fluid to enable them to visualize the flow patterns experimentally.

In the range of finite Froude and moderate Reynolds numbers, the literature on the subject is somewhat fragmented. On the experimental side, Deblor & Fitzgerald (1968), and Deblor (1973) were among the first to report on investigations of low- and moderate-Reynolds-number flows at finite Froude number. Some of their photographs have been widely cited and reproduced. It must be noted, however, that other observed flow behaviour which they reported (e.g. the non-axisymmetric attached-vortex regime discussed below) has not been given the notice it deserves. Unfortunately, both reported studies were lacking in the experimental detail that is necessary to calculate adequately the Froude numbers of a number of the cited flow situations.

Although there have been numerous other experimental studies concerned with stratified flow past a sphere, a systematic presentation of the variation of characteristic flow patterns with Fi , Re has not been delineated clearly. Experiments of Mason (1977) and Lofquist & Purtell (1984) demonstrated that the drag coefficient is influenced by the presence of stratification. In their experiments, for $Fi \lesssim 3$, the drag coefficient was increased by as much as 25% over the corresponding homogeneous case at the same Re owing to lee-wave drag effects. For $Fi \gtrsim 3$, the drag coefficient was decreased owing to turbulence suppression in the wake. (It is important to note that drag and other flow phenomena are also Reynolds number dependent.) Further experiments on the drag on two- and three-dimensional obstacles have been conducted recently by Castro, Snyder & Baines (1990). Lofquist & Purtell (1984) also report measurements of both horizontal and vertical separation angles in their flows as a function of Fi , where the lee-wave suppression of separation is quite apparent. These authors also provide a number of shadowgraphs delineating flow observations, particularly in the turbulent flow regime; these experiments are incorporated on our flow-regime diagram.

Hanazaki (1988) presented numerical calculations on flow patterns and internal wave fields for flows at a fixed $Re = 200$ and internal Froude numbers (our definition: note that Hanazaki defined the Froude number in terms of the sphere radius while in the present study the diameter is used) in the range $0.125 \leq Fi \leq 100$. The Hanazaki study revealed the important role of internal wave structure on the near flow field, specifically in the potential for complete suppression of a separated region in the lee of the sphere and in the alteration of the pressure and velocity fields by the wave structure. For $Fi \lesssim 0.2$, the Hanazaki flows are approximately two-dimensional and are in qualitative agreement with Drazin's (1961) three-dimensional, low- Fi theory. Because Hanazaki's calculations were limited to a single Re and $Fi \geq 0.125$, the study covered only a very limited region of dimensionless parameter space, and thus did not address many of the phenomena inherent to the general problem of linearly stratified flow past a sphere.

The dividing streamline height H_s is the vertical coordinate $z = \pm H_s$ of the upstream streamlines along $y = 0$ that will just pass over or under the sphere and is a useful concept in the discussion of stratified flows. Drazin (1961), in a nonlinear theory, determined H_s as

$$\frac{H_s}{\frac{1}{2}D} = 1 - 2\alpha Fi, \quad (1.1)$$

where α is a constant. Hanazaki's (1988) numerical predictions for α range from $0.8 \leq \alpha \leq 1.2$. Sheppard (1956) determined an estimate of $2H_s/D$ based on a very simple physical hypothesis. He postulated that a fluid parcel could rise over a hill only if it had sufficient kinetic energy upstream of the obstacle to overcome the potential energy required to raise the parcel from its upstream elevation to the top of the hill. Sheppard's prediction for the normalizing dividing streamline height H^* is

$$H_s^* = \frac{H_s}{\frac{1}{2}D} = 1 - 2Fi, \quad (1.2)$$

which is the same as Drazin's (1961) result with $\alpha = 1$. Hanazaki's (1988) results roughly support Sheppard's formula. Hunt & Snyder (1980) and Castro *et al.* (1983) investigated stratified flow over three-dimensional obstacles giving particular attention to the dividing streamline height concept and to the formation of internal waves. In a follow-on study, Snyder *et al.* (1985) confirmed the validity of Sheppard's

(1956) formula for a range of roughly axisymmetric hill shapes and a variety of stable density profiles. Snyder *et al.* (1985) suggested that further work was needed to determine firmly the limits of applicability of the modelling experiments.

For certain regions of parameter space, lee waves are found downstream of obstacles in stratified flows. Crapper (1959), using a linearized wave equation, estimated the normalized lee wavelength λ/D for a three-dimensional obstacle, which for the sphere reduces to

$$\frac{\lambda}{D} = 2\pi Fi, \quad (1.3)$$

along the plane $y = 0$.

Honji (1987) reported on four separate experiments at different Fi, Re combinations. His observations were made in the horizontal plane of symmetry and are in good agreement with the flow categorizations presented below; his experiments are also included on our flow-regime diagram. Honji did not systematically vary Re and Fi , as we have done.

Motivated by potential applications to the flow past individual mountain peaks in the Earth's atmosphere (e.g. see Berger & Wille 1972) and oceans, Brighton (1978) conducted a series of experiments in a closed-circuit stratified water channel on the flow past bottom-mounted truncated cylinders, hemispheres and cones. Brighton's studies considered Froude numbers (based on obstacle heights) from 0.03 to 0.3 and Reynolds numbers (based on base diameter) from 100 to 1000. For these parameter ranges he found the flows to be approximately two-dimensional (i.e. horizontal) except near the tops of the obstacles. For sufficiently large Froude numbers, Brighton found cowhorn-shaped eddies with horizontal axes in the obstacle lee at the elevation of the top of the obstacle. He observed vortex shedding at sufficiently large Re provided $Fi \lesssim 0.15$ (our definition). The shedding frequency was found to be the same at all heights; i.e. the vortices had vertical coherence. The Brighton findings are also in agreement with the present studies. Because of the rather thick boundary layer on the floor of his water channel (i.e. his upstream conditions were not uniform), Brighton's experiments have not been incorporated on our flow-regime diagram.

The near-wake structure of a sphere in a stratified flow has recently been studied in a series of experiments by Chashechkin & Sysoeva (1988), Sysoeva & Chashechkin (1988) and Chashechkin (1989). These authors reported that when the separation line on the sphere is projected on a vertical cross-stream plane, a rectangle in a certain Froude number range is formed; i.e. the cross-section of the wake is approximately rectangular.

Interest in the behaviour of stratified turbulent wakes has motivated a considerable amount of study of higher-Reynolds-number flows past bluff bodies. The review article by Lin & Pao (1979) summarizes many of the results of that effort. The process of generation, evolution and decay of the turbulent wake has been examined in some detail. The very striking evolution of almost two-dimensional vortex structures at large distances downstream of the disturbance has been noted by many researchers. These 'pancake' vortices or coherent structures evolve from a turbulent near wake which collapses because of the presence of background stratification. The evolution of the large scales into such well-defined horizontal structures suggests that there is periodic large-scale vortical motion in the near wake which does not decay as rapidly as the small-scale turbulence in the near wake collapsing mixed region (Hopfinger 1987).

In §2, the experimental facility and experimental techniques employed are discussed. In §3, the experimental observations of the various characteristic flow

patterns are discussed and placed on an Fi, Re flow-regime diagram. As each characteristic flow is discussed, various quantitative measures of the flow observations along with scaling analyses to describe the physics of the various phenomena observed are also included. A summary and concluding remarks are given in §4.

2. Experimental facility and techniques

The experiments were conducted independently in tow-tank facilities located at the University of Wyoming (UW) and at Arizona State University (ASU). Each facility has a computer-controlled towing carriage mounted on rails along the tank walls to translate model obstacles and experimental accessories along the tank axis. The carriages can be operated in a time-dependent translational mode but in the present experiments only steady speeds were employed. The tanks are filled with a linear stratification using salt-stratified solutions by the well-known Oster (1965) two-tank method. The density profiles were measured by either removing fluid samples and measuring the density with a refractometer or by using traversing conducting probes.

Owing to the zero-buoyancy-flux boundary condition along the free surface and along the tank bottom, and owing to evaporation, the linear density gradients near these boundaries are destroyed with time. The desired linear profiles are maintained approximately by adding fresh water daily along the free surface and introducing appropriate amounts of salt crystals along the tank bottom.

In the UW experiments two towing arrangements were employed; (i) a towing wire, which extended the entire length of the channel, and (ii) a sting support, where each body was supported by a thin tapered rod which was attached at the body's aft end. A discussion of the two towing methods is contained in the Appendix. A series of studies was performed with each towing arrangement; however, only the results and observations of the sting-support studies are reported here. The sting support used a stiff 27 cm long rod, whose diameter tapered from 0.64 cm to 0.2 cm. The rod was supported by a thin symmetrical airfoil which led to the towing carriage above the channel.

In the ASU experiments, the model spheres were supported by taut nylon cord (0.03 cm diameter) or steel wire (0.05 cm diameter) passing through the sphere centre. One end of the cord or wire was connected to a point above the water level and toward the front right-hand side of the towing carriage. The other end was attached to the bottom of a thin knife-edged plate rigidly attached to the left-hand rear side of the carriage and reaching to a level approximately 0.5 cm above the tank floor. The support wire orientation was thus at an angle of about 17° from the tank centreline. This method of supporting the models eliminated the 'sag' that would have occurred by a wire oriented along the channel axis. Furthermore, the boundary layers that would grow along the wire for a streamwise orientation were also eliminated (see the Appendix). During the experiments, sphere vibrations were negligible over the entire speed range investigated. Time exposures of the sphere, for example, for periods as long as 60 s indicated no blurring of the sphere image. Furthermore, for the experiments conducted, there was no evidence of the support wire significantly affecting the flow in its near wake. Further support for this conclusion is that the UW experiments and the ASU experiments are in agreement.

A variety of flow-visualization techniques including shadowgraphs, neutrally buoyant tracer particles, dye tracers and reflective flakes were used extensively in

these studies. Observations were made routinely from both horizontal and vertical perspectives. Both 35 mm still and video photography were used.

Shadowgraph images for both horizontal and vertical planes were obtained by directing a high intensity arc lamp source through a condensing lens onto a Fresnel lens which produced uniform parallel light through horizontal or vertical sections of the channel. Images on a Mylar sheet on the opposite side of the channel were then photographed, usually with some slight observation angle in order to avoid the camera being in a direct line with the light source. The basic three-dimensionality of the density structure cannot be determined from the images produced by these techniques: the sharpness is degraded, *vis-à-vis* the images in Boyer *et al.* (1989), and the density structure inferred by these images is an integrated cross-sectional value. The need for a minimum of two viewing planes is thus essential. The density gradients for the low Fi , low Re experiments for the sphere were so weak that the shadowgraph technique could not be employed effectively. This is in contrast to the cylinder experiments for which excellent shadowgraphs could be obtained at small Fi , Re combinations; see, for example, figure 3 of Boyer *et al.* (1989).

Polystyrene beads of nominal diameter 0.05 cm and density $1.040 \pm 0.005 \text{ g cm}^{-3}$ were used as tracer particles. The natural density variation of the particles and background density distribution employed were such as to give a quite uniform particle distribution in the tank. Particle streak photographs were taken in either horizontal or vertical cross-sections by illuminating the tracer particles by a plane light-sheet approximately 0.5 cm wide. The light source and camera were either fixed to the carriage or to the tow-tank. As for the shadowgraphs, particle streak images for three-dimensional motions are more difficult to interpret than their two-dimensional counterparts. Because the light sheet is quite thin, the three-dimensional motions, especially in vertical cross-sections off the centre plane, tend to advect tracer particles into and out of the sheet. The particle streak approach of obtaining the approximate velocity fields in horizontal and vertical cross-sections thus provides only limited quantitative information for such three-dimensional flows. As will be noted, however, their use is an excellent method for obtaining qualitative information on characteristics of a given flow field.

Fluorescein dye (ASU) and reflective flakes (UW) were also used for flow visualization. The reflective flake particles were supplied in a suspension of isopropyl alcohol, which enabled an easy resuspension in a salt-water solution which matched the mean density of the water surrounding the object. The particles were small enough to stay in suspension for a period of hours, although the specific gravity of the particles was of the order of 3. Overnight, the particles dropped out of suspension, so a new set of tests could be made without the contamination of the previous day's experiments. In these methods the tracers were introduced in the vicinity of the upstream stagnation point, prior to translating the sphere. The experiments were then initiated by engaging the carriage and the flow field illuminated by the light-sheet. Photographs were taken after the flow became fully developed.

Density profiles in the ambient fluid and in the sphere wake regions were measured (ASU) using vertically traversing microscale-conductivity probes. The probe speeds were of the order of 25 cm s^{-1} so that the density profiles, so obtained, were approximately instantaneous. The parameters considered in the experiments are given in table 1.

Parameter	UW	ASU
D (cm)	1.27, 1.905, 2.54, 3.81, 5.08	0.95, 1.905, 3.175, 3.81, 5.08
Tank dimensions		
L (cm)	10	12.2
W (cm)	30	40
H (cm)	20	22–25
D/H	0.063–0.254	0.05–0.23
N (s ⁻¹)	1.1–1.4	0.66–1.48
U (cm s ⁻¹)	0.05–5.0	0.05–18
Re	5–3 × 10 ³	25–10 ⁴
Fi	7 × 10 ⁻³ –2.5	10 ⁻² –15

TABLE 1. Experimental parameters

3. Experimental observations and measurements

The first objective of the experimental programme was to describe and categorize the qualitative nature of various characteristic motions observed in the internal Froude and Reynolds number ranges attainable with the present facilities; i.e. $0.005 \leq Fi < 20$ and $5 \leq Re < 10\,000$. The observational techniques used to make these determinations were shadowgraph, particle streak, dye tracer and reflective flake photographs. Figure 2 is a Fi against Re flow regime diagram showing the Fi, Re combinations studied (a minimum of one experiment for each data point) and the designated flow type observed; these various characteristic flows will be described further below. The UW and ASU experiments are designated by lower and upper case letters, respectively. The dashed lines represent the approximate boundaries between each flow type. Transitional experiments, for which there was some uncertainty in categorizing the flow, are indicated by a tilde above the flow designation symbol. The experiments of Lofquist & Purtell (1984) and Honji (1987) are also included. The present observations are in good agreement with their results.

Summary qualitative sketches for each of the characteristic flows are given in figure 3. Here we have noted the principal large-scale features of the respective motions by focusing on the flow fields observed along streamwise-oriented horizontal and vertical planes, both piercing the centre of the sphere, respectively.

As each characteristic flow is discussed qualitatively, various quantitative measures of flow-field observables will be made and compared with available theories or scaling arguments. These comparisons lead to a better understanding of the physical processes of importance in each of the characteristic flows and, additionally, provide a means for comparing future analytical or numerical models with the physical experiments. Let us now describe the characteristic flows by proceeding in the general direction of small to large Fi, Re combinations in figure 2.

3.1. Steady two-dimensional attached vortices (a, A)

For $Fi \lesssim 0.2$ and $Re \lesssim 70$, and both parameters limited from below by the capabilities of the experimental facilities (i.e. see table 1), one obtains a flow for which the characterizing feature is a steady attached vortex on the lee-side of the sphere. Figure 4 is reflective flake photograph for an experiment at $Fi = 0.009$, $Re = 19$; as can be noted the separation region in the sphere lee (arrow) is relatively small, but nevertheless unmistakable; no cases of unseparated flow were observed in the current experimental programmes. We term this characteristic flow as a 'steady two-dimensional attached vortex' (symbols a, A on figure 2). Figures 5(a), 5(b) and

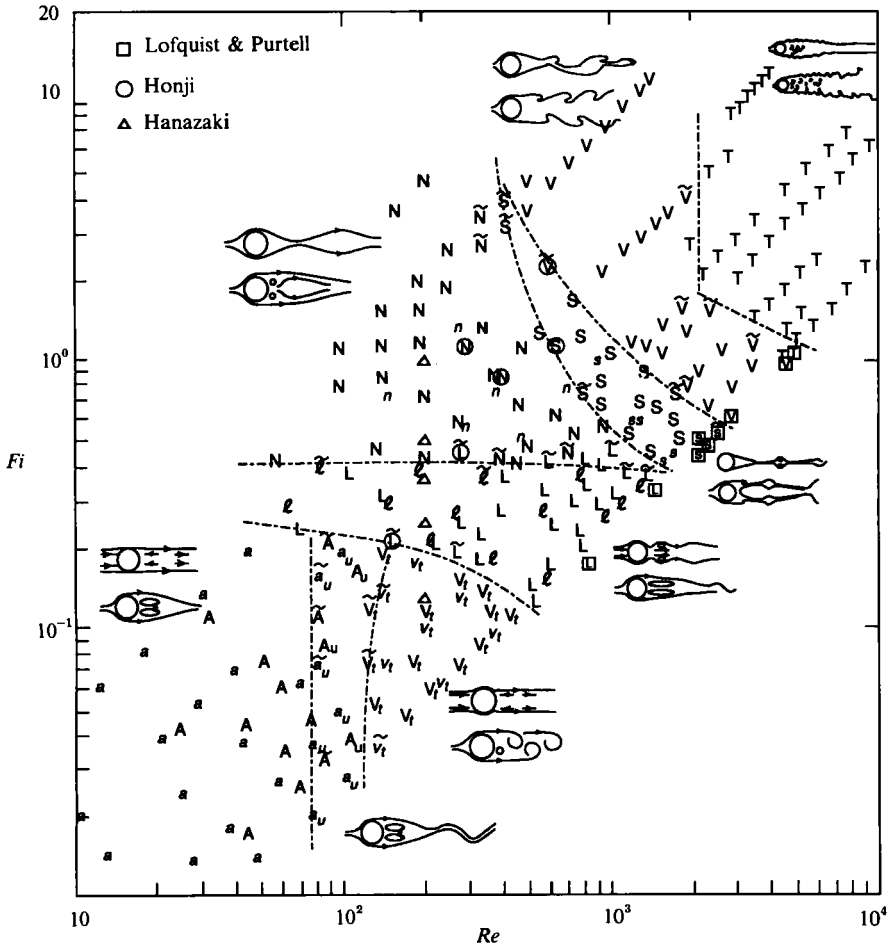


FIGURE 2. Flow regime diagram; Fi vs. Re .

5(c) are, respectively, a dye tracer photograph in the ($z = 0$)-plane, a particle streak photograph in the same plane and a particle streak photograph in the ($y = 0$)-plane for the same flow regime. Figure 5(d) is an interpretive sketch of the wake region for this regime. The attached vortex is two-dimensional in the sense that at each observation level z , the vertical motion is weak owing to the importance of stratification at small Fi and to the fact that the Re is not large enough to generate strong vertical motions for particles passing over the sphere. The fact that the vertical motion is very weak is clearly evident in figure 5(c). Note that the normalized dividing streamline height based on (1.2) for the experiment of figure 5(c) is $H_s^* \approx 0.95$; figure 5(c) shows clearly that very little vertical motion occurs upstream of the sphere.

Figure 5(a) is a photograph of the envelope of a fluorescein dye tracer released upstream of the sphere; the observer sees a vertical projection so that the outer boundary of the bubble region is presumably along the streamwise centreplane, $z = 0$. The term bubble is used herein interchangeably with the lee-side attached vortex region. The left to right upward directed white line is the light reflection from the sphere support wire; the wire is visible in many photographs and will not again be noted. Figure 5(a) shows clearly that the flow separation point is somewhat


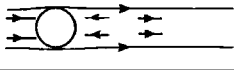

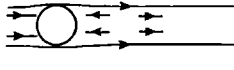
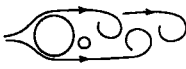
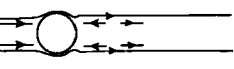


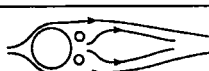
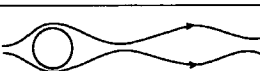
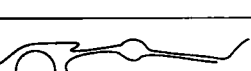


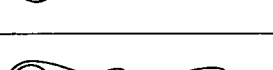
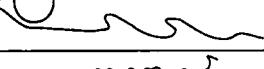

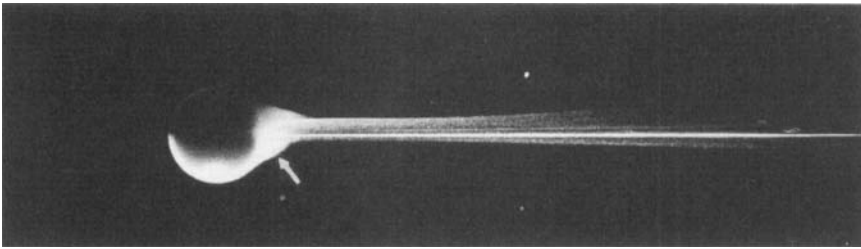
Regime	Horizontal centre plane	Vertical centre plane
A, a steady two-dimensional attached vortices		
A_u, a_u unsteady two-dimensional attached vortices		
V_v, v_t two-dimensional vortex shedding		
L, l lee-wave instability		
N, n non-axisymmetric attached vortex		
S, s symmetric vortex shedding		
V non-symmetric vortex shedding		
T turbulent wake		

FIGURE 3. Interpretive sketches of flow regimes.

FIGURE 4. Steady two-dimensional attached vortices (a, A); reflective flake photographs, $Re = 19$, $Fi = 0.009$ and $D/H = 0.19$. The arrow indicates the separated bubble region.

downstream of the maximum sphere dimension in the streamwise centreplane. Note that the attached two-element vortex nature of the lee-side flow is clearly evident; no unsteadiness or suggestion of vortex shedding is in evidence. The stagnation streamline continues as the streamwise centreline in the sphere lee. Horizontal dye tracer photographs at elevations z in the range $0 \leq z \leq H_s$ indicate a small decrease in the lee-side bubble size with height.

Figures 5(b) and 5(c) are particle streak photographs for experiments in which the light sheet is oriented along the ($z = 0$)- and ($y = 0$)-planes, respectively. Figure 5(b) is in agreement with figure 5(a), showing a double eddy structure in the sphere lee

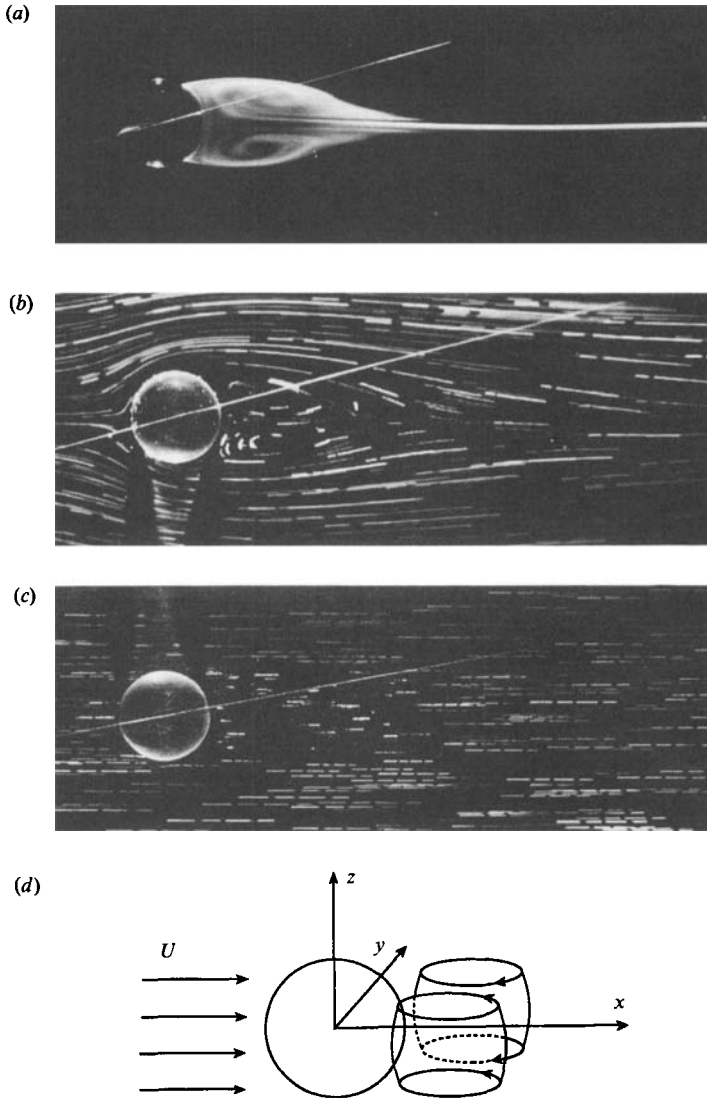


FIGURE 5. Steady two-dimensional attached vortices (a, A); (a) dye tracer along horizontal centreplane, $z = 0$; $Re = 63$, $Fi = 0.03$, $D/H = 0.18$; (b) particle streaks along $z = 0$; $Re = 63$, $Fi = 0.05$, $D/H = 0.18$; (c) particle streaks in vertical centreplane $y = 0$; $Re = 83$, $Fi = 0.03$, $D/H = 0.23$; (d) interpretive sketch of lee-side eddies. The total exposure time for the photograph in (b) is $t_e = 40$ s which corresponds to a normalized exposure time $\tau_e = t_e(U/D) = 1.72$ based on the advective timescale D/U . The light beam has been chopped so as to define the flow direction from short streak to long streak. The corresponding values for (c) are $t_e = 40$ and $\tau_e = 1.22$; in this photograph the particle streak has been chopped three times at approximately equal increments of time.

along $z = 0$. The dark regions 'below' the sphere on figure 5(b) (i.e. $y < 0$) are due to the refraction of the light sheet which has its orientation toward $-y$. Note also that no significant blocking is in evidence immediately ahead of the sphere. This is in sharp contrast to the horizontal circular cylinder situation at small Fi as discussed by Boyer *et al.* (1989) and is due to the fact that, in the sphere case, particles can go around the obstacle.

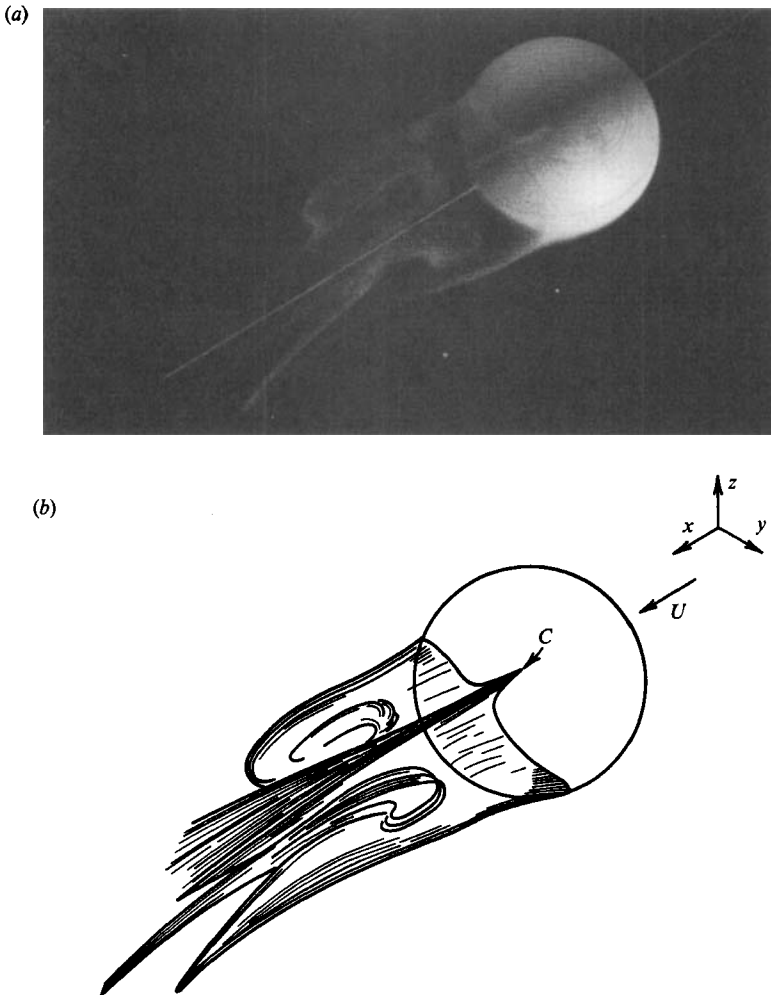


FIGURE 6. Oblique view of unsteady two-dimensional vortices (a_v, A_v) from slightly behind the sphere on the downstream side; (a) reflective flake photograph and (b) interpretive sketch; $Re = 54$, $Fi = 0.015$, $D/H = 0.25$. The cusp-like separation line on the sphere is indicated as point C . The towing wire method was used in this example (see Appendix).

Figure 5(c) demonstrates that the vertical motion is exceedingly weak in this flow regime in the ($y = 0$)-plane and such observations hold for other streamwise vertical planes as well. The observations that the lengths of the particle streaks in the lee of the sphere in figure 5(c) can vary considerably, even for neighbouring particles, is due to the fact that fluid particles in the attached eddies have non-zero y -velocity components and thus are continually advected in and out of the light-sheet; while ideally the y -velocity component along $y = 0$ should be zero, the fact that the light-sheet is approximately 0.5 cm thick leads to observations of particles with non-zero y -velocity.

Figures 6(a) and 6(b) are, respectively, an oblique angle photograph of an experiment using reflective flake particles and an interpretive sketch for an experiment at $Fi = 0.015$ and $Re = 54$. The photograph shows the separation bubble in the sphere lee as well as depicting the line of separation on the sphere. Note the flattened ellipsoidal nature of the bubble region, owing to stratification effects, and

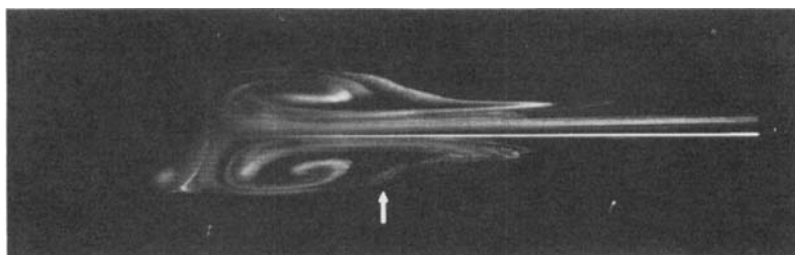


FIGURE 7. Unsteady two-dimensional attached vortices (a_u, A_u); reflective flake photograph of horizontal centreplane $z = 0$, $Re = 126$, $Fi = 0.036$, $D/H = 0.25$. The arrow indicates the unsteady distortion of the separation envelope.

the cusp-like separation line (point C on figure 6*b*) as one moves to the polar regions (top and bottom) of the sphere. Above this separation line on the sphere's surface, a very thin, vertical sheet of particles is visible in the downstream fluid. This region is where the horizontal flow remains attached to the sphere and converges in the neighbourhood of the ($y = 0$)-plane. The separation envelope itself is a vortex sheet, which presumably continues to be connected during the roll-up process, until it is dissipated by viscosity. Vertical shadowgraph observations do not reveal density distortions, which is in agreement with the limitation to horizontal motions at these low Fi experiments.

3.2. Unsteady two-dimensional attached vortex (a_u, A_u)

Beginning at $Re \approx 70$, time-dependent, horizontal distortions of the wake envelope begin to appear. These wave-like distortions originate near the separation line and propagate downstream to the trailing end of the envelope and collect at the trailing end; see figure 7. This characteristic flow is delineated as an 'unsteady two-dimensional attached vortex' (symbols a_u, A_u , on figure 2). Very little, if any, vorticity is released to the downstream flow by these disturbances, although a regular, sinuous trail of particles is formed downstream. The disturbances have been observed to occur simultaneously on both sides of the envelope. They are also reasonably periodic, although no quantitative measurements of the periodicity were made. Taneda (1956), in his study of low-Reynolds-number flow past cylinders, referred to these distortions as 'gathers', and found their presence starting at $Re \approx 35$ up to $Re \approx 150$, where the very distinctive vortex-shedding process was observed to commence. This regime is similar to the unsteady attached vortex regime for a right circular cylinder in a homogeneous fluid; see, for example, the photographs in Batchelor (1967). Similar patterns were also observed by Boyer (1968) for flows in the lee of a right circular cylinder in the presence of background rotation.

The dependence of the normalized bubble length, $\Delta b/D$ (see figure 8) on the Reynolds number in the steady and unsteady two-dimensional attached vortex regimes was investigated by focusing on observed particle streak flow patterns in the ($z = 0$)-plane (see figure 5*b*) for the ASU experiments and reflective flake photographs (see figure 7) for the UW experiments. Figure 8 is a plot of the observed $\Delta b/D$ data against Re for the steady and unsteady two-dimensional vortex regimes. Given that Fi varies from 0.02 to 0.20, one notes a good collapse of the data, independent of Fi . The scatter of the data increases with Re because of the increased difficulty of defining the bubble length for unsteady flows. Note that there is a systematic difference between the UW and ASU bubble-length measurements. This is attributed to the different flow-observation techniques employed. The ASU particle measure-

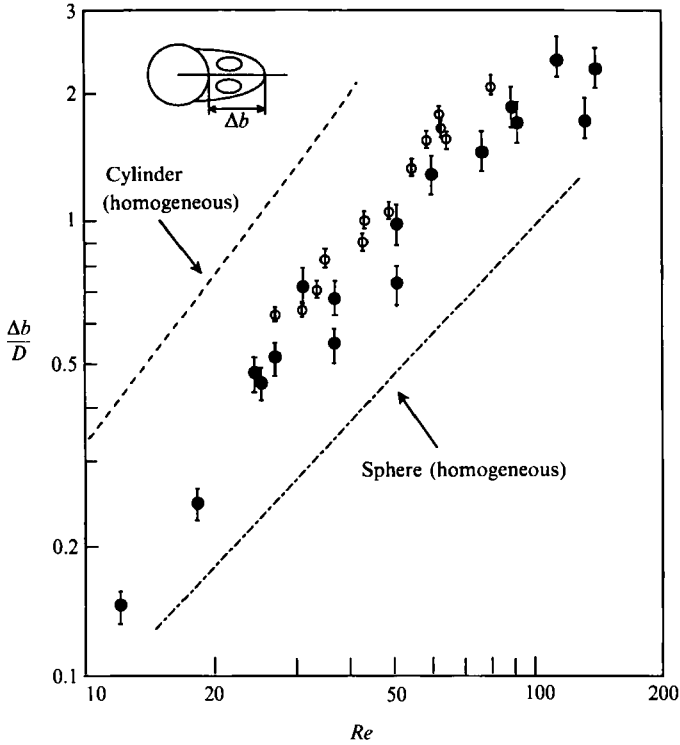


FIGURE 8. Normalized bubble length, $\Delta b/D$ against Re for steady and unsteady two-dimensional attached vortex regimes; ---, homogeneous flow past a long circular cylinder (Churchill 1988); -.-, homogeneous flow past a sphere from Taneda (1956). ●, UW experiments; ○, ASU studies.

ments of $\Delta b/D$ were larger because the critical streamlines identified were those that circumscribed the bubble region. The larger uncertainty bands for the UW data are due to the instantaneous photographic observations of bubble size, which were then averaged over multiple photographs.

The experimental relation for $\Delta b/D$ against Re for a sphere in a homogeneous fluid, as obtained by Taneda (1956) and that for a two-dimensional cylinder in a homogeneous flow, are also plotted on figure 8. Because stratification inhibits flow over the sphere tending, as discussed above, to a more two-dimensional motion, the separation bubble is larger at a given Re for the stratified as compared to the homogeneous case; the bubble length, however, is less than that for a right circular cylinder. The bubble length is independent of Fi because the stratification is strong enough in all experiments in these regimes to inhibit vertical motion, thus making the normalized bubble size depend primarily on Re .

For the sphere, the data indicate an approximately linear increase of normalized bubble length $\Delta b/D$ with Re . This dependence can be predicted from scaling arguments. Consider the x -momentum and conservation of mass equations in the vicinity of the ($z = 0$)-plane. Neglecting vertical motions and variations with z , one can write

$$u \frac{\partial u}{\partial x} + v \frac{\partial u}{\partial y} = -\frac{1}{\rho_0} \frac{\partial p}{\partial x} + \nu \left(\frac{\partial^2 u}{\partial x^2} + \frac{\partial^2 u}{\partial y^2} \right), \quad (3.1)$$

$$\frac{\partial u}{\partial x} + \frac{\partial v}{\partial y} = 0, \quad (3.2)$$

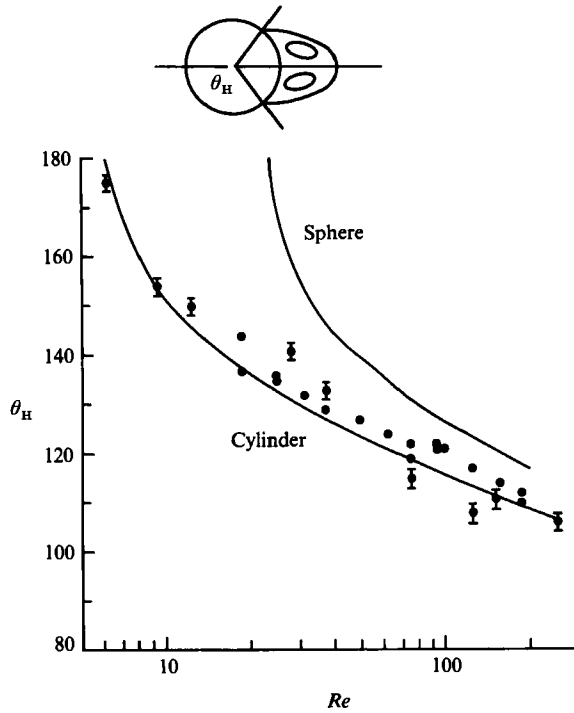


FIGURE 9. Horizontal separation angles, θ_H , for $Fi \lesssim 0.2$, as a function of Re . The separation angles for homogeneous flow past spheres and long circular cylinders, as summarized by Churchill (1988), are shown as solid lines.

respectively, where (u, v) are the velocity components along (x, y) . Assume that in the bubble region $u \sim U$, $\Delta x \sim \Delta b$ and $\Delta y \sim D$. Equation (3.2) then yields $v \sim UD/\Delta b$. If one then hypothesizes that inertia balances transverse viscous diffusion in (3.1), one finds

$$\frac{\Delta b}{D} \sim \frac{UD}{\nu} = Re. \quad (3.3)$$

The results of figure 8 support this scaling argument. At $Re \gtrsim 100$ for this regime, the bubble region becomes increasingly unsteady and one is beginning to enter another flow regime.

Additional observables of interest in the steady and unsteady attached vortex regimes are the separation angles as observed in the vertical and horizontal planes and as represented by the greatest extent of separation in each of these observation planes. The separation angle is defined as the angle from the upstream centreline to the separation point. For the horizontal plane, the maximum separation angle always occurs on the equatorial plane, independent of the flow regime. The linear stratification field, together with the axisymmetry of the sphere, would suggest symmetry of this type.

If flow regimes are confined to those below the lee-wave instability regime (i.e. $Fi \lesssim 0.2$ as discussed below), the influence of the internal wave field is diminished and the flow is predominantly horizontal. For these regimes, the measured horizontal separation angles at the equator are shown in figure 9 as a function of Re . Owing to the dominance of stratification, these separation angles are independent of Fi throughout this range of parameter space. For comparison, the separation angles for

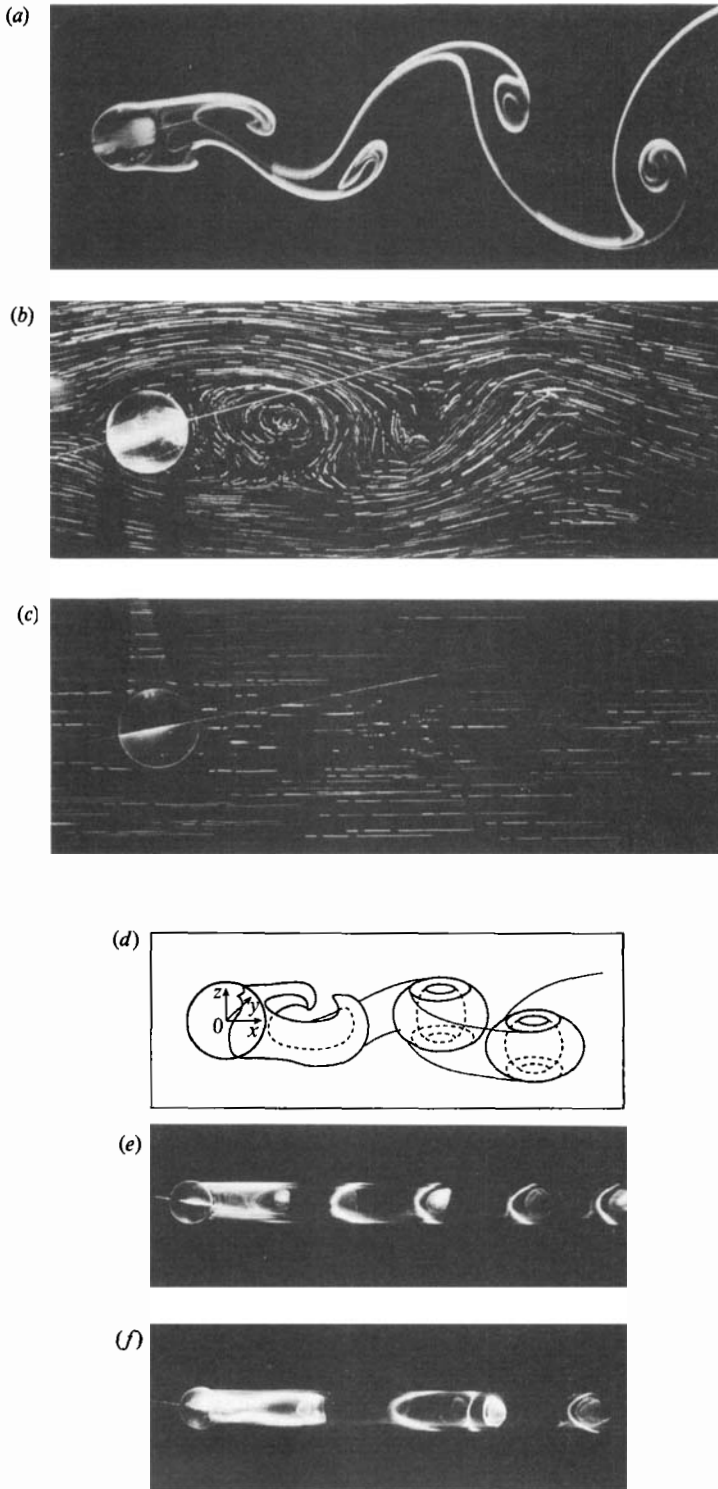


FIGURE 10. Two-dimensional vortex shedding (v_r, V_r); (a) dye tracer along horizontal centreplane, $z = 0$; $Re = 180$, $Fi = 0.05$, $D/H = 0.23$; (b) particle streaks along $z = 0$; $Re = 200$, $Fi = 0.09$,

the homogeneous flow past spheres and cylinders are also shown. This maximum separation angle closely follows the separation angle behaviour of the flow past a cylinder in a homogeneous flow. The observed two-dimensional, vertically coherent nature of the flow would suggest this type of behaviour. Additionally, the experimental value of Re for incipient separation (i.e. ≈ 6) follows the cylinder's incipient separation value ($Re \approx 6.2$). Data on the dependence on horizontal ($z = 0$ plane) and vertical ($y = 0$ plane) separation angles as a function of Fi and Re will be given in figures 31 and 32, respectively.

3.3. Two-dimensional vortex shedding (v_v, V_t)

For $Re \gtrsim 120$ and $Fi \lesssim 0.15$ (see figure 2), vortices of characteristic thickness $2H_s$ and approximately two-dimensional over the range $-H_s \lesssim z \lesssim H_s$ are shed alternately from the sphere; this flow regime is termed 'two-dimensional vortex shedding' (symbols v_v, V_t on figure 2) and is exemplified by the dye tracer photograph in the ($z = 0$)-plane and particle streak photographs in the ($z = 0$)- and ($y = 0$)-planes, in figures 10(a)–10(c), respectively. Figures 10(a) and 10(b) show clearly the alternate shedding of eddies with vertically oriented vorticity; these experiments are at approximately the same Fi, Re . Furthermore, the shedding phase is approximately the same in both photographs. The sphere diameter in both experiments is the same, but in the interest of showing more of the far wake, the field of view in figure 10(a) has been expanded. The dye tracer photograph shows a classical vortex street signature. Note, however, from the particle streak photograph that only the near wake vortices are very active, while the far wake vortices are dominated by the mean flow.

The vertical particle streak photograph of figure 10(c) shows clearly that the vertical motions in this regime, again owing to the small Fi and relatively small Re , are weak. The normalized dividing streamline height is $H_s^* \approx 0.82$ and again it is noted that only weak vertical motions are in evidence upstream of the sphere. The question then arises as to the vertical dependence of the horizontal streamline patterns and in particular the frequency of the eddy shedding since the 'local obstacle diameter' varies with height. To answer this question, a series of experiments were conducted in which a dye tracer was released along the full surface of the sphere. Figure 10(d) is a schematic representation of the qualitative nature of the character of the vortex-shedding structure as obtained from these experiments. Figures 10(e) and 10(f) are photographs of the dye tracer patterns observed from vertical streamwise oriented light-sheets along the sphere centreplane ($y = 0$) and along the sphere tangent-plane ($y = -\frac{1}{2}D$). These photographs show clearly that the vortex shedding is vertically coherent.

The Strouhal number $St = \omega_e D/U$, where ω_e is the eddy-shedding frequency from one side of the sphere, was measured by hot-film anemometry and by using dye-tracer flow observations. Figure 11 is a plot of St against Re for all of the experiments conducted in this regime; the Froude number varied in the range $0.03 \lesssim Fi \lesssim 0.28$ (which extends beyond the present flow regime). The results show clearly that the Strouhal number St is independent of both Fi and Re with $St \approx 0.20$. Also plotted are the cylinder (Roshko 1953) and sphere (Achenbach 1974) results for homogeneous flow; note that our findings closely follow those for the cylinder.

$D/H = 0.23$; (c) same as (b) except view is for vertical centreplane; (d) schematic diagram of three-dimensional nature of vortex shedding phenomena; and (e), (f) photographs of dye tracers released from full sphere as made visible in planes along $y = 0$ and $y = -\frac{1}{2}D$, respectively. The parameter values for (e) and (f) are $Re = 180$, $Fi = 0.06$ and $D/H = 0.21$.

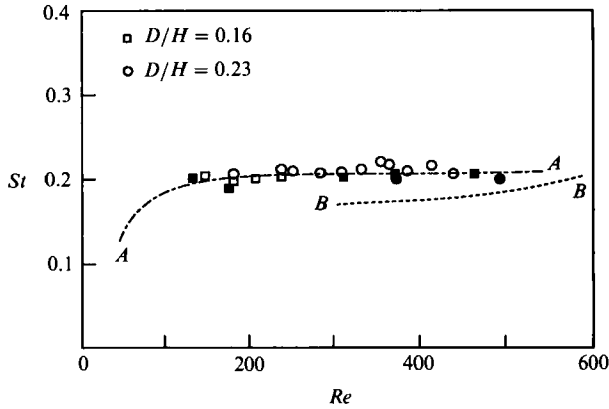


FIGURE 11. Strouhal against Reynolds number for two-dimensional vortex shedding; *A-A* Roshko (1953) for cylinder in homogeneous flow; *B-B* Achenbach (1974) for sphere in homogeneous flow; open symbols are used for ASU experiments and solid symbols for UW experiments.

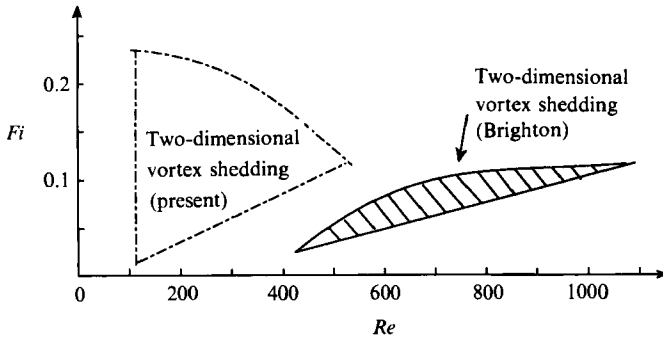


FIGURE 12. Comparison of regime diagram observations for two-dimensional vortex shedding between Brighton's (1978) results for a hemisphere and the present experiments.

Brighton (1978) reported similar phenomena for a hemisphere mounted on the lower horizontal plane surface of his stratified water tunnel; i.e. he indicated that vortex shedding occurred at Reynolds numbers in the range $400 \lesssim Re \lesssim 700$, depending on the internal Froude number. These Reynolds numbers were based on his free-stream flow with the hemisphere being embedded in a bottom boundary layer of thickness not significantly less than the hemisphere radius. These bottom boundary layers lead to a significantly different flow upstream of the obstacle and explain the rather large differences in Reynolds numbers at which these regimes are observed in the two experiments. The differences in the Fi, Re regions of parameter space between Brighton's (1978) observations of two-dimensional vortex shedding and those found herein are delineated on figure 12.

Hanazaki's (1988) smallest Fi calculation was at $Fi = 0.125$ (his Froude number 0.25) and $Re = 200$, as denoted by a triangle on figure 2. The present laboratory experiments demonstrate that, under these conditions, two-dimensional vortex shedding occurs. Hanazaki's calculation led to a steady solution, however, in which a large recirculating eddy structure of characteristic streamwise dimension $\approx 4D$ was found in the lee of the sphere. Referring to figure 8, our results show that when the lee bubble length reaches about $2D$, unsteadiness in the wake begins to appear. Possibly, Hanazaki's downstream boundary condition of $\partial u / \partial x = 0$ at the outflow boundary precluded vortex shedding.

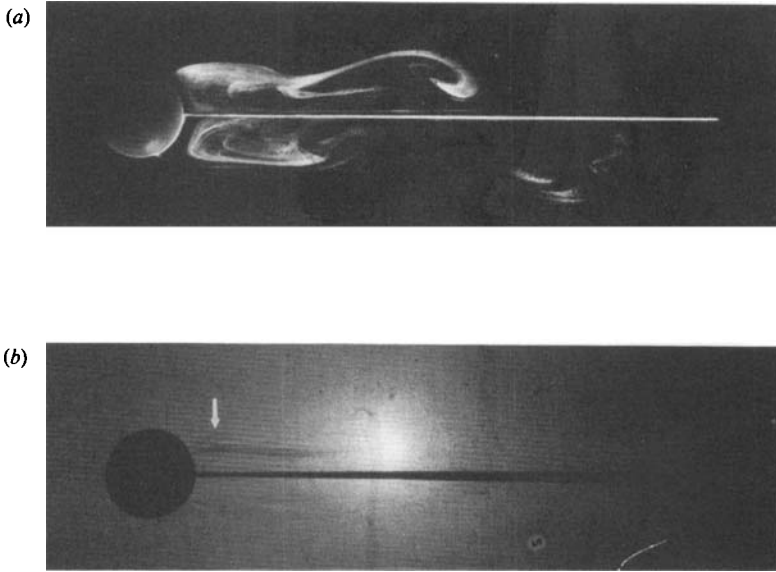


FIGURE 13. Transition flow from two-dimensional vortex shedding (v_v, V_v) to lee-wave instability (ℓ, L); (a) reflective flake photograph in ($z = 0$)-plane; (b) shadowgraph in ($y = 0$)-plane; $Re = 380$, $Fi = 0.18$, $D/H = 0.19$. The arrow indicates the rotor location.

3.4. Lee-wave instability (ℓ, L)

As the Froude number is increased at fixed Re , lee waves in the vicinity of the streamwise vertical centreplane $y = 0$ become increasingly evident. The transition to the higher Fi regime, termed lee-wave instability from the two-dimensional vortex-shedding regime is a gradual one. In this transition region the first lee-wave crest appears to be unstable but vortex shedding in the neighbourhood of the streamwise centreplane continues to higher Fi (as was noted in the measurements of St in the previous section). Such a transition flow is exemplified by the reflecting flake and shadowgraph photographs of figures 13(a) and 13(b), respectively.

In the Froude number band $0.2 \lesssim Fi \lesssim 0.4$, the width being somewhat dependent on Re , and for the range of Reynolds numbers considered, $60 \lesssim Re \lesssim 1500$ (see figure 2), the first lee-wave crest was found to be unstable, exhibiting overturning motions. Figure 14 contains particle path and shadowgraph photographs depicting typical flow patterns for this regime termed, 'lee-wave instability' (symbols ℓ, L on figure 2). In addition to overturning motions this regime is also characterized by (i) a steepening of the vertical density gradient along the top and bottom of the separation envelope boundary and (ii) a narrowing of the separation line on the sphere; these features can be noted on the shadowgraph of figure 14(c). This is the same regime termed 'cow-horn eddies' or 'rotors' by Brighton (1978). Fluid particles above the dividing streamline and in the vicinity of $y = 0$ rise over the top of the sphere and descend into a deep trough on the downstream side. Owing to the strong vertical shear in the vicinity of the first lee-wave crest, overturning takes place as is clearly evident in figures 14(b) and 14(c).

The vorticity equation can be written as

$$\frac{D\omega}{Dt} = (\omega \cdot \nabla) \mathbf{v} + \frac{\nabla \rho \times \nabla p}{\rho^2} + \nu \nabla^2 \omega, \quad (3.4)$$

where $\omega = \nabla \times \mathbf{v}$ is the vorticity, D/Dt is the substantial derivative and \mathbf{v} is the

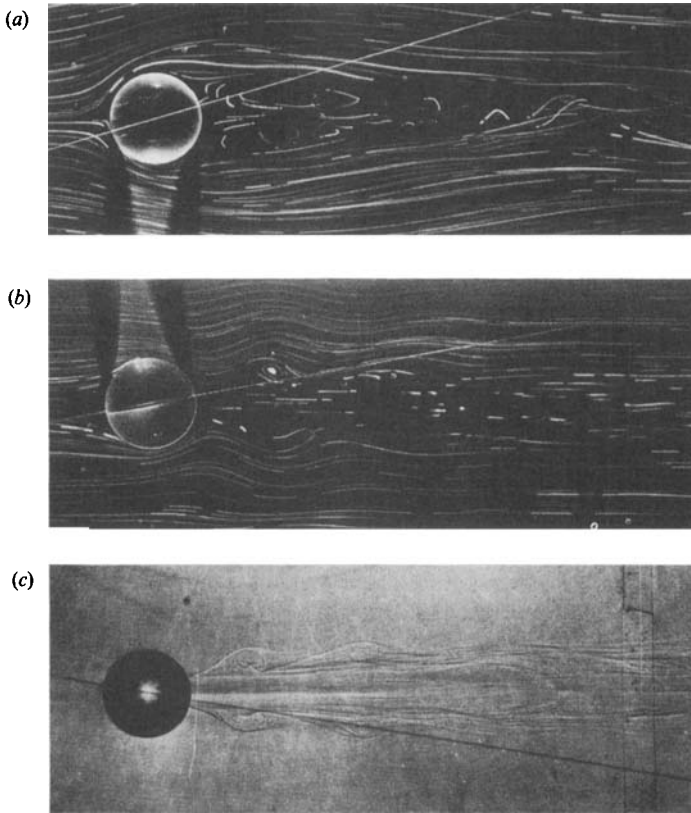


FIGURE 14. Lee-wave instability (ℓ, L); (a), (b) particle streak photographs in ($z = 0$)- and ($y = 0$)-planes, respectively; $Re = 500$, $Fi = 0.19$, $D/H = 0.23$; (c) shadowgraph for $Re = 700$, $Fi = 0.26$, $D/H = 0.23$.

velocity. From (3.4) one notes that baroclinic effects are important in the generation of vorticity and, in the present context, play a role in the phenomenon of lee-wave instability. The baroclinic vorticity production term $(\nabla\rho \times \nabla p)/\rho^2$ in the vicinity of $y = 0$ under the Boussinesq approximation becomes

$$\frac{\nabla\rho \times \nabla p}{\rho^2} \approx -\frac{g}{\rho_0} \nabla\rho \times \mathbf{k} \approx \frac{g}{\rho_0} \frac{\partial\rho}{\partial x} \mathbf{j}. \quad (3.5)$$

On the upstream side of the lee-wave crest, $\partial\rho/\partial x > 0$, showing that the baroclinic effect tends to form an overturning motion.

Figures 15(a) and 15(b) are density profiles taken through the first lee-wave crest region in the vicinity of $y = 0$ for two different Fi, Re combinations. These profiles delineate clearly the locations of the edges of the overturning regions, showing that the density profile is statically unstable. These so-called rotor regions lead to patches of small-scale turbulence; see figure 14(c).

The horizontal centreplane particle streak photograph of figure 14(a) shows that the wake pattern at this level contains a two-dimensional vortex pair with the flow near the streamwise centreline being advected back toward the sphere. This two-dimensional flow in the centreplane was found to be unsteady far downstream, as can be noted on figure 14(a).

In the lee-wave instability flow regime, fluid parcels approaching the sphere at

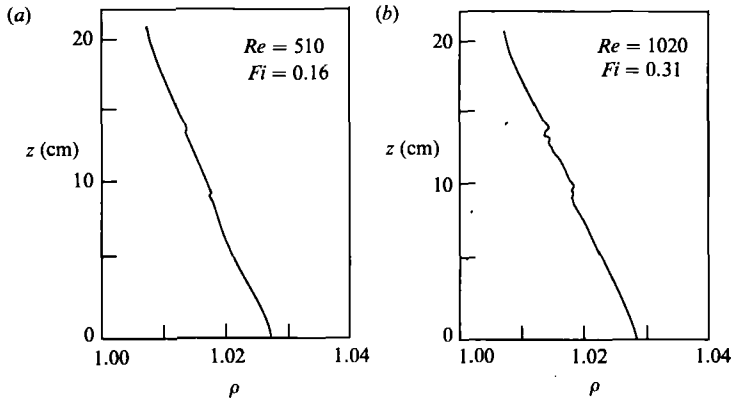


FIGURE 15. Density profiles across the top and bottom rotors in the ($y = 0$)-plane for lee-wave instability experiments.

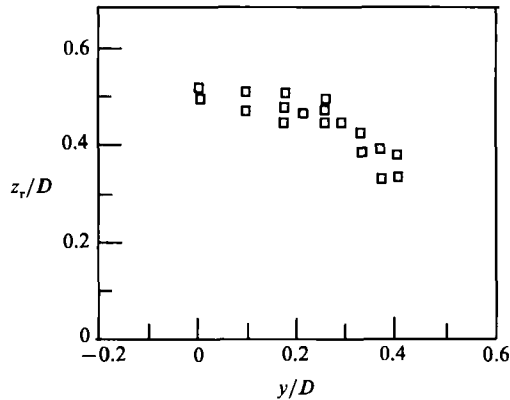


FIGURE 16. Normalized height of lee-wave crest against y/D (lateral position); $Re = 520$, $Fi = 0.16$, $D/H = 0.24$.

elevations $|z| \gtrsim H_s^*$, in the vicinity of $y = 0$ say, had sufficient kinetic energy to go over (or under) the sphere; note that $H_s \approx 0.6$ for the experiments of figure 14, in approximate agreement with Sheppard's formula (1.2). After reaching the crest, buoyancy effects increase the downflow behind the crest, which tends to delay flow separation in a vertical cross-section along $y = 0$; see figure 14(b). The lee waves die out further downstream owing to viscous dissipation and radiative effects.

For fluid parcels approaching the sphere at $|z| < H_s$, there was a tendency for motion in horizontal planes at the parcel's upstream flow level. The adverse pressure gradient experienced by fluid particles in the immediate lee of the sphere caused flow separation in horizontal planes as indicated for the ($z = 0$)-plane in figure 14(a). The flow in the region $|z| \lesssim H_s$ is thus approximately two-dimensional with the lee-side separated wake region being a vertically deformed separation bubble.

Detailed observations of experiments in this regime indicated that the lateral extent of the overturning region was less than that of the sphere diameter. Traversing conductivity probe measurements such as given in figures 15(a) and 15(b) were used to obtain measures of the height of the rotor regions. Figure 16 is a plot of the normalized height of the lee-wave crest, z_r/D , against y/D for $Re = 520$, $Fi = 0.16$, $D/H = 0.23$. Note the decrease in thickness with y/D , with no rotor

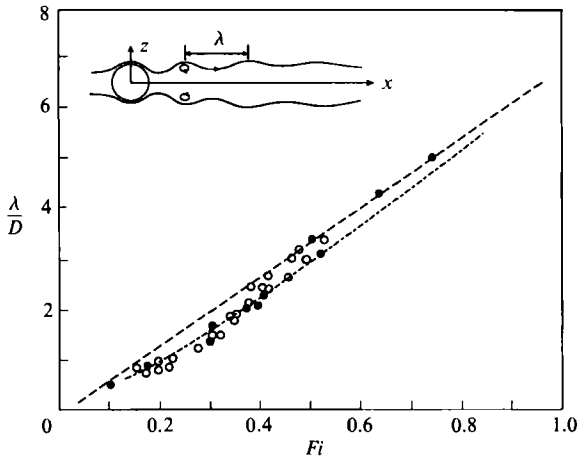


FIGURE 17. Normalized lee wavelength against Fi : ---, linear theory of Crapper (1959); — · —, Hanazaki's (1988) calculations; solid symbols from UW experiments and open symbols from ASU studies.

appearing for $y/D \gtrsim 0.4$. The rectangular-shaped lee-wave instability region, reported by Sysoeva & Chaschchkin (1988), was not observed in the present studies.

The linear theory of Crapper (1959), predicts that the normalized lee wavelength λ/D is a linear function of Fi and is given by (1.3) for the vertical centreplane; i.e. along $y = 0$. Lee wavelengths were measured from both particle streak photographs and shadowgraphs. Measurements were made of the distance between the first and second crests at the approximate elevation of $z = \frac{1}{2}D$. The results are plotted in figure 17. The measurement error of λ/D is relatively higher at lower Fi because the wavelength is small compared with the sphere diameter. The results indicate clearly that the measured wavelengths are systematically smaller than that predicted by linear theory. Similar results have been found by Chomaz *et al.* (1990).

Hanazaki (1988) provided numerical results for experiments at $Re = 200$ and $Fi = 0.25, 0.35$ (his figures 3(e) and 3(d), respectively) which should both lie within the lee-wave instability regime. Generally, there is good qualitative agreement between the flow patterns found by Hanazaki and those observed in the current experiments. This includes such observables as the general nature of the flow field including in particular the motion in the horizontal and vertical centreplanes. His results for the prediction of the normalized lee wavelengths as indicated on figure 17 are in good agreement with our observations. One feature not predicted by the Hanazaki numerical experiments are the rotor regions which are clearly evident in the physical experiments.

With increasing Fi , the lee waves increase in amplitude, and both the vertical and horizontal separation angles tend toward the aft centreline with, as a limiting case, little or no separation in the vertical; i.e. see figure 18. The limiting case defines lee-wave resonance. Similar flow patterns were reported by Honji (1987); e.g. see his figure 1(b). Inhibition of separation accompanies reduced pressure and so must occur in both horizontal and vertical planes, with convergence of constant density surfaces immediately behind the sphere. The horizontal dimension of the separation region also decreases with decreasing Re . The very narrow separation envelope is connected to one or more bulges directly downstream. The interior of these bulges is strongly vortical and structured. The size of these bulges can vary from almost unobservable to close to the same size as the object.

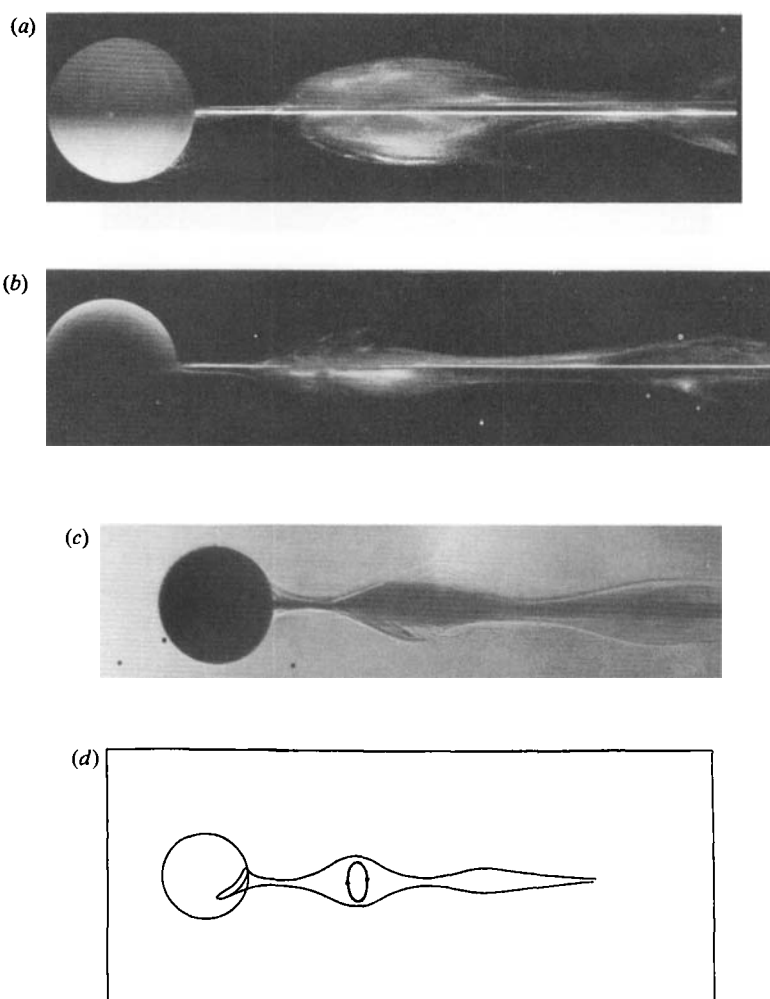


FIGURE 18. Transitional flow between lee wave instability (\mathcal{L} , \mathcal{L}) and non-axisymmetric attached vortex in (n , N) regimes; $Re = 859$, $Fi = 0.43$ and $D/H = 0.13$; (a) reflective flake photographs along horizontal centreplane, $z = 0$; (b) reflective flake photograph along vertical centreplane, $y = 0$; (c) side-view shadowgraph; and (d) interpretive sketch. The closed directed line on (d) represents the vorticity within the isolated structure.

The very narrow region in Fi where this resonance is observed to occur would suggest that this characteristic motion represents the transition between the two adjacent regimes. The value of Fi of this transitional flow is approximately 0.4, which is consistent with the arguments of Lofquist & Purtell (1984), where their energy arguments led to an estimate for Fi of 0.35 at this interval wave resonance point. Their argument is an inviscid one, which is justified by examining the flow-regime diagram, where this transitional flow is independent of Re .

3.5. Non-axisymmetric attached vortex (n , N)

For certain ranges of Re for homogeneous flow past a sphere, an axisymmetric vortex is attached to the lee side of the obstacle. Buoyancy effects modify this general flow regime for the stratified case. For $Fi \gtrsim 0.4$ and for a range of Reynolds numbers, as indicated on figure 2, the flow is characterized by a double wake structure, which is

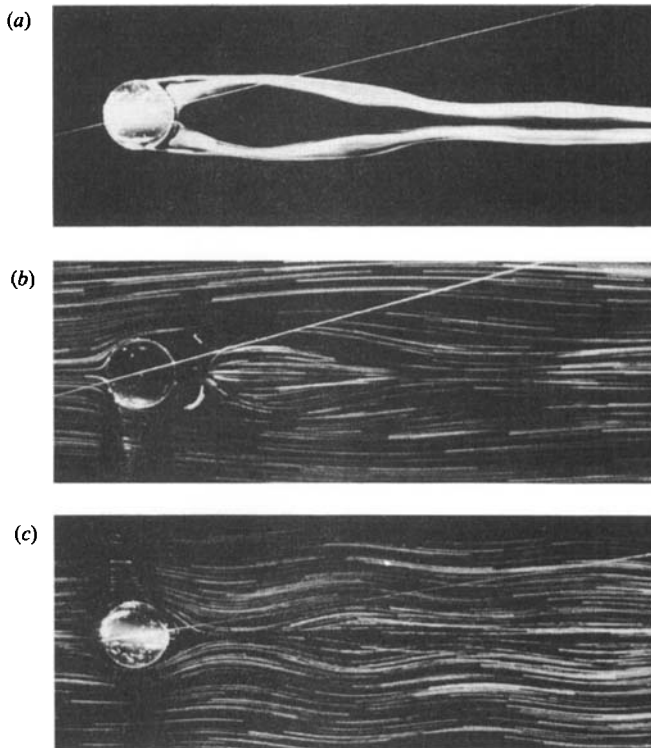


FIGURE 19. Non-axisymmetric attached vortex (n, N); $Re = 480$, $Fi = 0.68$, $D/H = 0.15$; (a) dye-tracer photograph along horizontal centreplane, $z = 0$; (b) particle streak photograph along $z = 0$; (c) particle streak photograph along vertical centreplane, $y = 0$.

termed a 'non-axisymmetric attached vortex' (symbols n, N on figure 2). Figures 19(a) and 19(b) are dye tracer and particle streak photographs, respectively, for the horizontal plane of symmetry $z = 0$, while figure 19(c) is a particle streak photograph for the vertical symmetry plane $y = 0$ to exemplify this regime.

Owing to the relatively larger internal Froude numbers for the experiments in figure 19, the measured dividing streamline height was $H_s \approx 0.25$; it appears that Sheppard's formula (1.2) is not valid at such large Fi . Thus, fluid parcels from relatively small $|z|$ have sufficient energy to pass over the sphere. This can be observed in figure 19(c). As seen in figure 19(c), a lee-wave pattern is in evidence far downstream of the sphere.

Figures 20(a) and 20(b) provide three-dimensional interpretive sketches of the attached vortical regions in the lee of the sphere. Conceptually, it may be clearer to examine this regime as Fi decreases towards $Fi \approx 0.4$. For weak stratification, the doughnut-shaped vortex ring is deformed in the vertical due to stratification; see figure 20(a). As the stratification increases the deformation increases, until at sufficiently large stratification, the deformed doughnut-shaped vortex is doubly reconnected, leaving two attached vortices, as in figure 20(b). As Fi is decreased below $Fi \approx 0.4$, the double wake structure disappears, and the attached eddies near $z = 0$ are elongated in the manner described for the lee-wave instability regime.

Figure 19(b) shows the presence of a horizontal bulge-like shape from one to three diameters downstream of the sphere. This region consists of fluid which is not part of the attached wake elements which are seen in figure 19(a). A schematic diagram

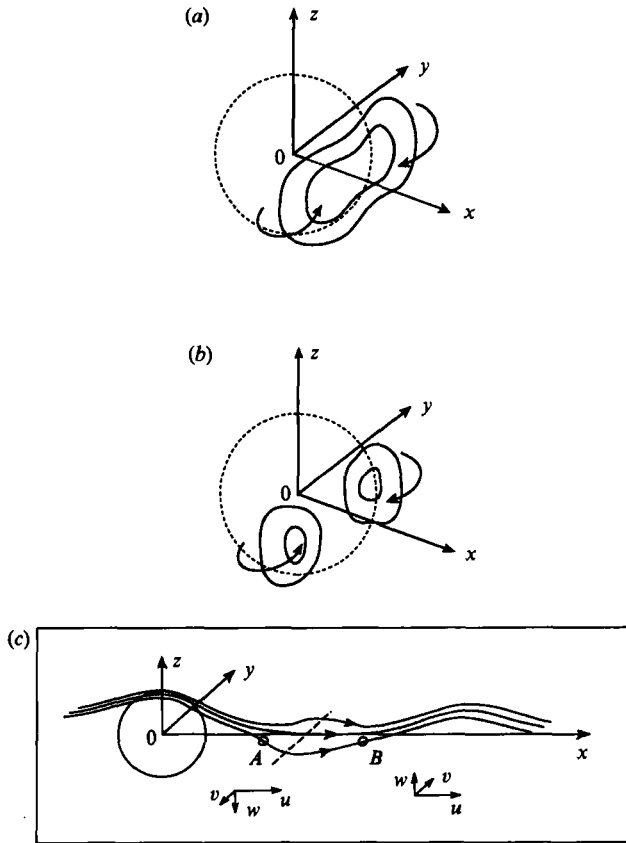


FIGURE 20. Interpretive sketches of the non-axisymmetric attached vortex for (a) weak stratification and (b) strong stratification. An interpretive sketch of the formation of the bulge-like particle streak pattern in the lee in the vicinity of the ($z = 0$)-plane is given in (c); see figure 19(b) and text.

showing how such bulge-like patterns near $z = 0$ are formed is given in figure 20(c). This figure depicts three neighbouring streamlines which pass over the sphere near $z = \frac{1}{2}D$ and $y = -\delta, 0$ and δ , where $\delta \ll D$. Fluid parcels pass over the sphere and attached lee-wave vortices (see figure 20a, b) and diverge horizontally on approaching the plane $z = 0$. They then rise again in the lee of the bulge. Note that the qualitative nature of the velocity components near A and B are indicated on the diagram.

A physical picture of the processes which contribute to the formation of non-axisymmetric attached vortices is presented below. We shall apply the concepts of surface topology, surface stress vectors, surface nodes and saddle points as discussed by Lighthill (1963) and Hunt *et al.* (1978). Briefly, the approach begins with the concept of surface stress (more precisely: strain rate) vectors, ϵ_w , in near-surface flows.

Very near the surface of an object, the velocity may be modelled by

$$U = \epsilon_w \xi_n, \tag{3.6}$$

where

$$\epsilon_w = \omega_w \times n = \frac{\tau_0}{\mu}, \tag{3.7}$$

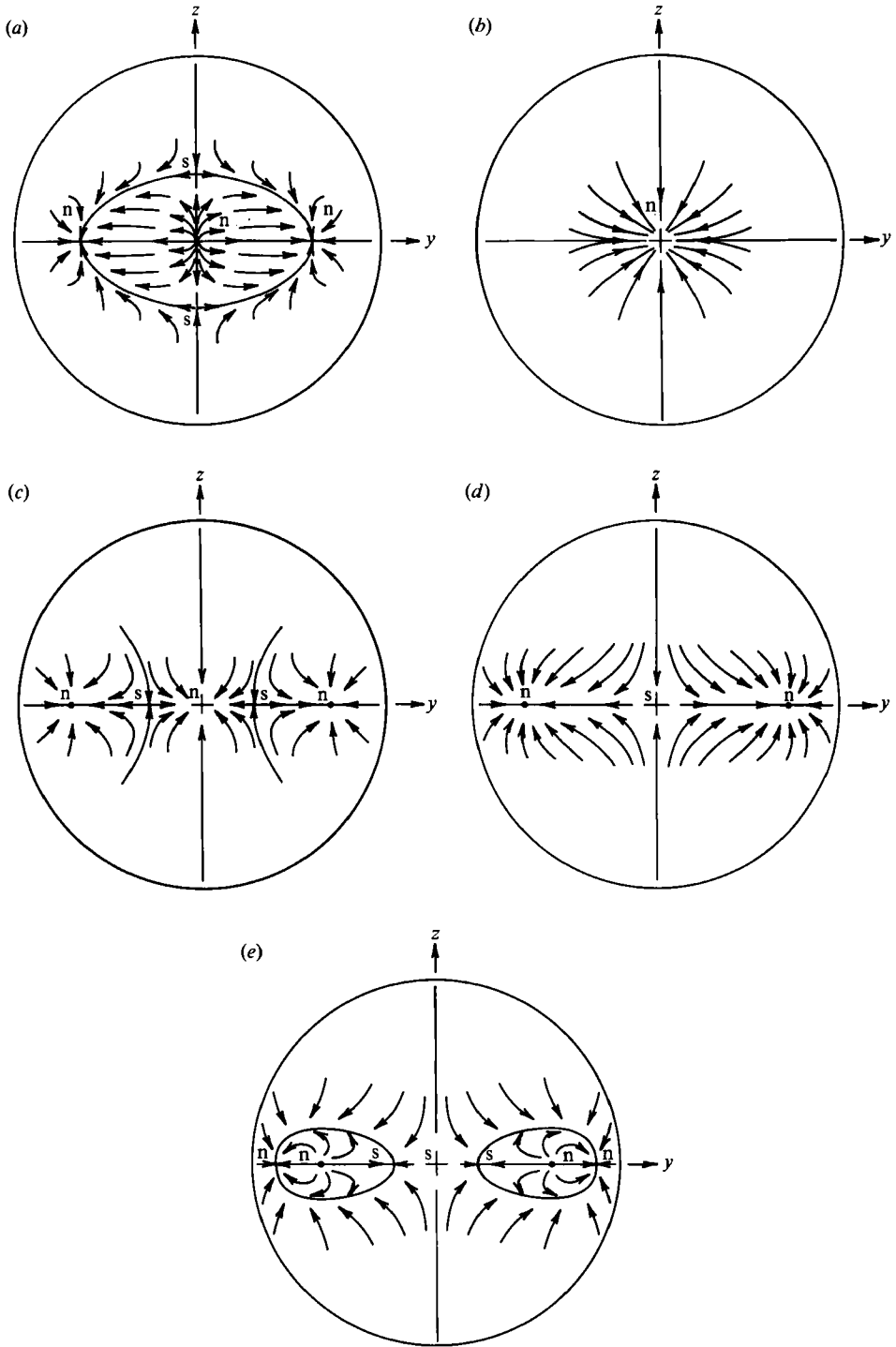


FIGURE 21. Topological patterns of surface stress lines, in the lee of the sphere, for the flow regimes leading to non-axisymmetric vortex flows. (a) Lee wave instability ($Fi < 0.4$), $n_n = 4$, $n_s = 2$; (b) limiting case for lee wave instability ($Fi \approx 0.4$), $n_n = 2$, $n_s = 0$; (c) transition flow between lee-wave instability and non-axisymmetric vortex flows, $n_n = 4$, $n_s = 2$; (d) incipient double node separation, $n_n = 3$, $n_s = 1$; (e) higher Fi flow, $n_n = 5$, $n_s = 3$.

ξ_n is the outward surface normal coordinate, ω_w the surface vorticity, \mathbf{n} the outward unit normal, $\boldsymbol{\tau}_0$ the surface stress vector and μ the viscosity. In this surface region, streamlines and surface stress lines are approximately aligned and the vortex lines are orthogonal to the surface stress.

At the edge of the viscous layer of thickness δ , the vorticity may be kinematically related to the velocity in this region as:

$$\int_0^\delta \omega \, d\xi_n = \mathbf{n} \times \mathbf{U}_0, \quad (3.8)$$

where \mathbf{U}_0 is the velocity at the edge of the viscous layer. The vortex lines, whose strength is the average vorticity across the boundary layer, are then orthogonal to the surface streamlines. The average convection velocity of boundary-layer vorticity is

$$\mathbf{U}_w = U_0^{-1} \int_0^\delta u \frac{\partial u}{\partial \xi} \, d\xi = \frac{1}{2} \mathbf{U}_0. \quad (3.9)$$

As has been discussed by Lighthill (1963), flows with mean velocity gradients in planes parallel to the surface cannot simultaneously satisfy relations (3.8) and (3.9) without the presence of positive surface streamwise vorticity. In regions of lower free-stream velocity, the surface vortex lines must therefore have a streamwise component, in order for the mean layer vortex lines to remain approximately orthogonal to the surface streamlines.

The basic characteristics of the surface stress lines, viewed from downstream, for the transition to non-axisymmetric wakes from the lee-wave instability regime, for increasing Fi , are sketched in figure 21. These patterns are reflective of the experimental observations of each of these flows. In each of the five cases shown

$$\sum n_n - \sum n_s = 2, \quad (3.10)$$

where n_n is the number of surface nodes and n_s is the number of saddles on the surface (the Poincaré–Bendixson theorem). The forward surface flow patterns are not shown in the figures. These forward regions will either possess one stagnation node or two stagnation nodes and one saddle point. (In either case, on the forward half, $\sum n_n - \sum n_s = 1$.) The basis for these patterns can be described as follows.

The fundamental premise in examining the formation of non-axisymmetric attached vortices is the separation criterion based on zero surface vorticity. Kinematically, the existence of zero surface vorticity would require the presence of one or more separation nodes on the surface of the sphere.

The flow calculations of Hanazaki for the distribution of isopycnals adjacent to the surface are particularly useful at this point. Hanazaki did not report the presence of the non-axisymmetric vortex flows, but we will take his isopycnal distributions to be indicative of the external wave field which exists prior to the separation process being discussed. It is assumed that the isopycnals are approximately representative of streamlines adjacent to the surface. The mean vorticity lines are thus approximately orthogonal to these isopycnals. For Hanazaki's case of $Fi = 0.35$ (his Froude number 0.7) the result is shown in figure 22(a, b). The convergence of the streamlines in the aft region of the equatorial plane indicates the higher velocities in that region compared to the velocities of the fluid which passes over (under) the sphere in the neighbourhood of $y = 0$. Owing to the need for positive streamwise layer vorticity in regions of lower external velocities, the surface vorticity is distorted in the vertical (in comparison to the mean vorticity), as is shown in figure 22(c).

Within the boundary layer, there are density gradients, particularly if the stratification is due to a low diffusivity scalar. This stratification within the boundary layer causes a diminishment of vorticity within the boundary layer itself, owing to baroclinicity, which must be adjusted for by a further increase in streamwise surface vorticity. The argument is briefly as follows, where we start with the general vorticity equation, under the Boussinesq approximation. With reference to figure 22, the y -component of vorticity, from (3.4) and (3.5), may be written as

$$\frac{D\omega_y}{Dt} = (\boldsymbol{\omega} \cdot \nabla) u_y + \nu \nabla^2 \omega_y + \frac{g}{\rho_0} \frac{\partial \rho}{\partial x}. \quad (3.11)$$

As was discussed in the context of lee-wave instability, $\partial \rho / \partial x < 0$ on the aft of the sphere and above the horizontal centreplane, owing to the isopycnal distortion in this region. This baroclinic term serves as an additional sink for vorticity (since $\omega_y > 0$). (A similar argument for the lower half of the sphere indicates that $\omega_y < 0$ and $\partial \rho / \partial x > 0$.) This deficit in vorticity must be compensated for by additional streamwise surface vorticity, which further distorts the central region of surface vortex lines, as is shown in figure 22.

The tendency of the surface vorticity lines to merge together in the central aft portion of the sphere is seen to create off-axis separation points on the equatorial plane as surface stress lines bifurcate, creating two nodal points and a central saddle point, as was illustrated in figures 21(b)–21(d) (through the sequence just described). This progression to the non-axisymmetric attached vortex regime may possibly proceed without baroclinicity, and be caused exclusively by the external wave field. A scaling of the convective and diffusive terms in the vorticity equation, however, indicates that the baroclinic term (if scaled by N^2) is quite comparable and should not be neglected.

With increasing Fi , the wake regions adjacent to the surface become larger and eventually merge into a single deformed vortex ring structure, as was shown in figure 20(a). At the larger Re boundaries of this regime, the wake becomes unsteady, and for sufficiently large Re, Fi the attached vortices begin to shed from the sides of the sphere.

3.6. Symmetric vortex shedding (s, S)

When the combination of Fi, Re is large enough (see figure 2), periodic vortex shedding is observed. The resulting flow patterns when viewed in either horizontal or vertical projections are symmetric and thus the term ‘symmetric vortex shedding’ (symbols s, S in figure 2) is used to describe this characteristic regime. Figure 23(a) is a vertically oriented shadowgraph and figure 23(b) a horizontal dye tracer photograph exemplifying this flow regime. Interpretive sketches of the wake flow corresponding to figures 23(a) and 23(b) are given in figures 24(a) and 24(b) respectively.

This regime has some similarities to the horse-shoe loop phenomenon discussed for the homogeneous case by Achenbach (1974). For homogeneous fluids the vortex loop shed from the sphere has no preferred direction with the separation point being a function of time. For the stratified case, however, vertical stability gives the phenomenon of the shedding of vortex loops a preferred direction; i.e. the geometric characteristics of each successive loop in the periodic process are similar on both sides.

Viewed in a vertical cross-section, the doughnut-shaped or split vortex structures as sketched in figures 20(a) and 20(b) respectively, shed from the sphere, grow slightly in the near wake, before collapsing in the far wake owing to stratification

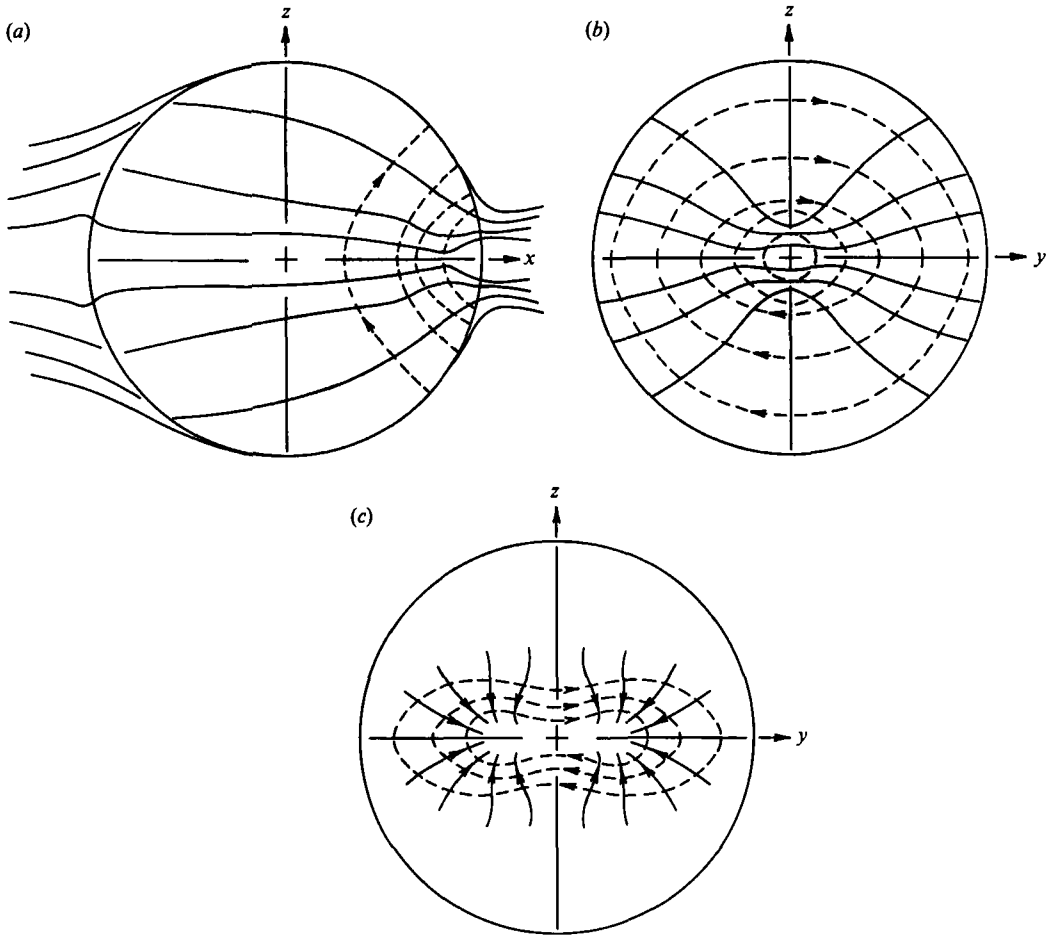


FIGURE 22. Sketches of general near-surface flow patterns and inferred vortex lines for $Fi \approx 0.35$, prior to formation of the double node separation points (similar to figure 21*b*). (a) Side view of ---, mean layer vortex lines, and —, streamlines at the edge of the viscous layer adjacent to the sphere. The streamlines are taken to correspond to the isopycnals of Hanazaki (1988), for $Fi = 0.35$. The streamlines within the fluid are for the ($y = 0$)-plane. The mean surface vortex lines are drawn orthogonal to the surface streamlines (equation (3.8)). (b) Aft view of the same parameters as (a); (c) aft view of —, the surface stress lines, and ---, surface vortex lines, showing the vertical distortion of the surface vortex line, as discussed in the text.

effects; see figures 23(a) and 24(a). The vortex loops, as viewed in a horizontal plane, shed in a symmetric fashion and gradually wrap-up becoming a single structure in the far wake following collapse. After collapse the structures merge and form a quasi two-dimensional alternating vortex street in the distant wake (not shown in figures 23 and 24).

The vortices on each side of the sphere, in this regime, can shed at slightly different times causing small asymmetries in the wake pattern. The flow regime is stable, however, in the sense that these asymmetries do not grow in the streamwise direction. The lifetime of the vortices generally increases with increasing Fi because at decreasing stratification levels, vortex collapse is delayed; owing to viscous effects by vertical shear, collapsed vortices decay more rapidly. In addition, at higher Fi ,

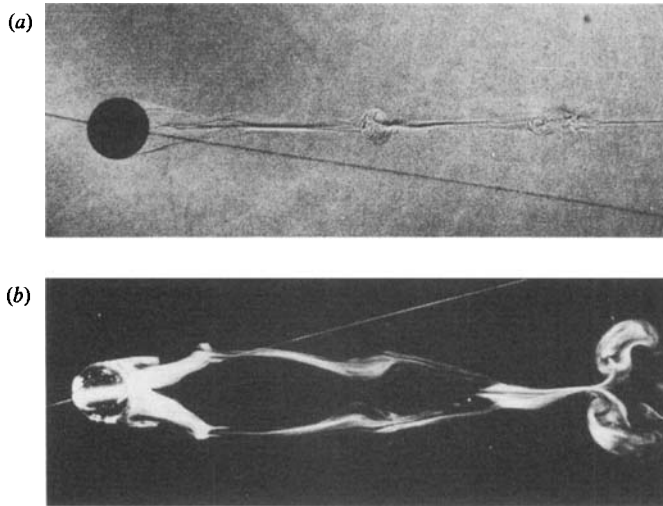


FIGURE 23. Symmetric vortex shedding (s, S); (a) side-view shadowgraph at $Re = 1120$, $Fi = 0.94$, $D/H = 0.15$; (b) dye-tracer photograph along horizontal plane of symmetry at $Re = 870$, $Fi = 0.86$, $D/H = 0.17$.

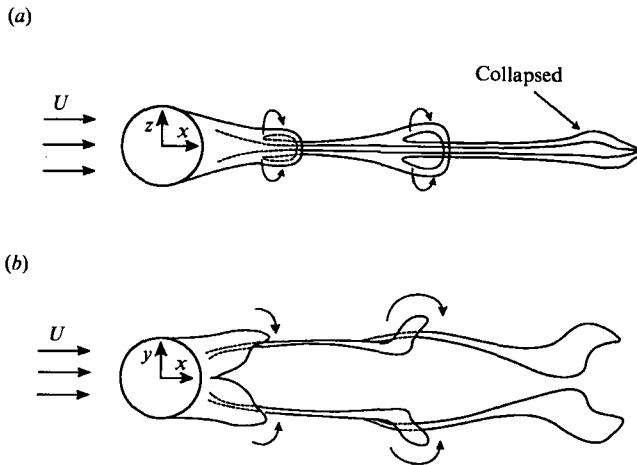


FIGURE 24. Interpretive sketch of vortex loops in the symmetric vortex shedding regime; (a) side view and (b) top view.

the vertical distortion of the doughnut-shaped vortex ring is relatively smaller and the suppression of the vertical scale is weak, thus leading to relatively taller vortices at higher Fi ; see figure 28.

The horizontal vorticity in the shed vortex 'rings' tends to advect lighter fluid downward towards the streamwise centreline from above and heavier fluid upward from below. This tends to leave a region of strong vertical density gradient variation along the streamwise centreline as is evidenced by the dark (and bright) lines between successive vortex loops as indicated in figure 23(a). The shedding frequency of the vortex loops, in particular the Strouhal number, was measured for a range of Re , Fi and these data are discussed below.

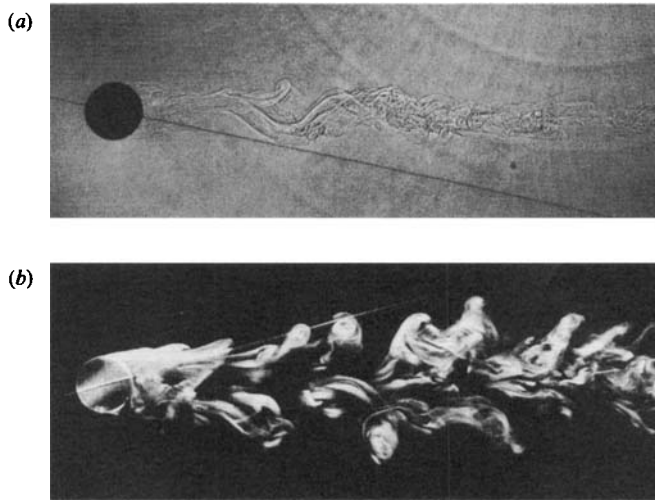


FIGURE 25. Non-symmetric vortex shedding (V); (a) side-view shadowgraph at $Re = 1550$, $Fi = 1.25$, $D/H = 0.17$; (b) dye-tracer photograph along the horizontal plane of symmetry for $Re = 1360$, $Fi = 1.38$, $D/H = 0.17$.

3.7. Non-symmetric vortex shedding (V)

As the Re , Fi combinations continue to increase, the wake becomes increasingly unstable and the vortex shedding gradually loses its symmetry. The vortices become highly three-dimensional with quasi-periodic shedding apparent in the horizontal centreplane $z = 0$. Figure 25(a) and 25(b) are, respectively, a vertical shadowgraph and horizontal dye tracer photograph ($z = 0$ plane) illustrating this flow regime which is designated as 'non-symmetric vortex shedding' (symbol V on figure 2). Note that the horizontal view demonstrates the quasi-periodic nature of the phenomenon but that this periodicity is not clearly evident in the vertical shadowgraph, where the wake oscillates, splits into small vortices and then collapses.

The near wake of the flow in this regime apparently consists of a low-level, turbulent attached bubble region. The periodic behaviour of the middle wake originates near the downstream portion of this attached bubble. The far wake is characterized by a thin collapsed turbulent region; see figure 25(a). The large difference in magnitude of the vertical and horizontal scales of the wake, as indicated in figures 25(a) and 25(b) respectively, are general characteristics of wakes in stratified flows; i.e. the vertical scale collapses and the horizontal one expands. This characteristic is enhanced as Fi is decreased.

At the largest Fi experiments in this regime, the shed vortex loops are similar to the horseshoe vortices described by Achenbach (1974). Achenbach reported that vortex loops begin to shed at $Re \approx 400$. The current observations indicate that vortex loop shedding begins at $Re \approx 380$ at high Fi (i.e. $Fi \approx 10$). Thus there is good agreement with Achenbach's results. Note from figure 2 that stratification tends to suppress vortex shedding; i.e. larger Re are required for shedding as Fi is decreased.

Measurements of the Strouhal number $St = \omega_e D/U$ for a wide range of Fi , Re were made in the symmetric and non-symmetric vortex shedding regimes; here ω_e is the shedding frequency from one side of the sphere. The shedding frequencies were determined from video tapes of experiments in which dye tracers and shadowgraphs were employed and from density records obtained from conductivity probes fixed in the wake.

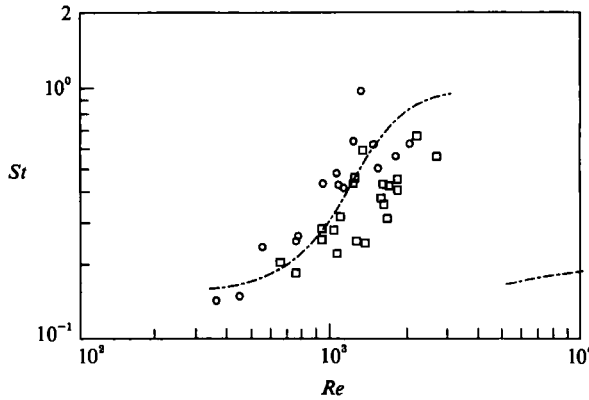


FIGURE 26. Strouhal against Reynolds number for \circ , the symmetric and \square , non-symmetric flow regimes; — —, Achenbach (1974) for a sphere in a homogeneous flow.

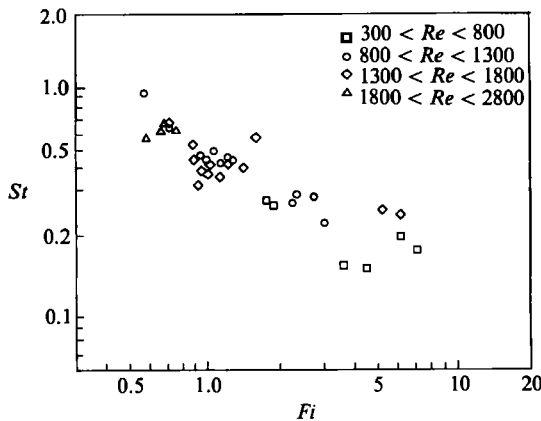


FIGURE 27. Strouhal against Froude number for various ranges of Re .

Figure 26 is a plot of St against Re for both the symmetric and non-symmetric vortex-shedding flow regimes. The results of Achenbach (1974) for a homogeneous fluid are also shown. Note that there is no strong distinction between the shedding frequencies of the two regimes. The stratified experiments have the same general trend of increasing St with Re as homogeneous flows. The observed variability of St for fixed Re , however, suggests the possibility of Fi effects. The data from figure 26 were also plotted as a St against Fi graph as shown in figure 27. The symbols in figure 27 represent various ranges of Re . This plot shows that there is a general decrease in St with an increase in Fi for each range of Re .

Shedding frequencies for higher Reynolds numbers were determined exclusively by conductivity probe measurements along the streamwise centreline at a distance $3D$ downstream of the sphere. For $Re \gtrsim 2000$, and for sufficiently large Fi , the higher frequency signal of the dominant mode had diminished to the point of being indistinguishable from the rest of the signal.

The normalized vertical height of the vortex structure δ_v/D in the symmetric and non-symmetric shedding regimes were measured using side-view shadowgraphs; here δ_v is the maximum vertical extent of the vortex structures. Measurements were made from a sequence of photographs prior to collapse and these are plotted against Fi in figure 28. The data suggest that $\delta_v/D \sim Fi^{1/2}$.

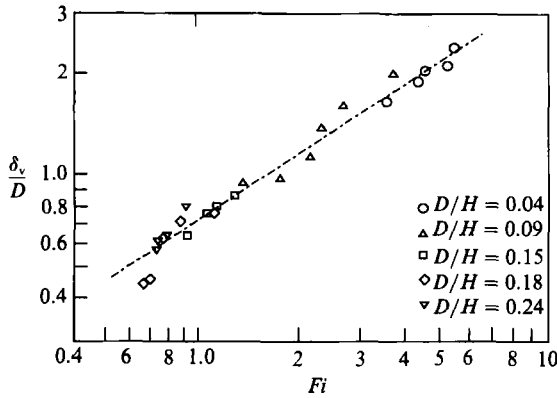


FIGURE 28. Normalized maximum vertical size of vortex structures for symmetric and non-symmetric vortex shedding regimes, δ_v/D against Fi .

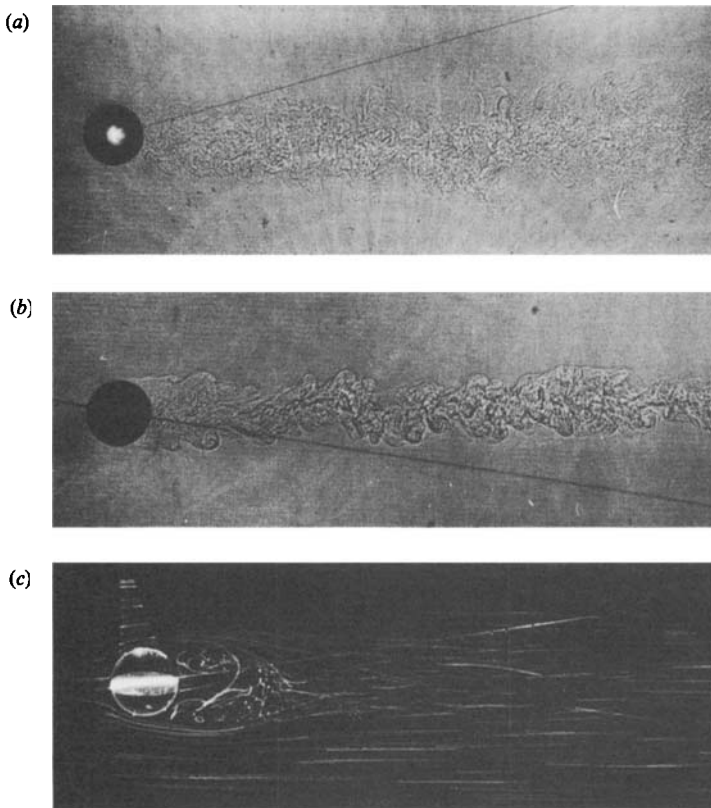


FIGURE 29. Turbulent wake (T); (a) top-view shadowgraph at $Re = 5100$, $Fi = 1.70$, $D/H = 0.23$; (b) side-view shadowgraph at $Re = 3810$, $Fi = 2.60$, $D/H = 0.17$; (c) particle-streak photograph for $Re = 4650$, $Fi = 4.10$, $D/H = 0.17$.

3.8. Fully-turbulent wake (T)

For sufficiently large Fi , Re combinations the wake appears to be fully turbulent, characterized by small-scale mixing; see figure 2. Figure 29 shows (a) a horizontal shadowgraph, (b) a vertical shadowgraph and (c) a $y = 0$ particle streak photograph exemplifying this flow regime termed 'fully-turbulent wake' (symbol T on figure 2).

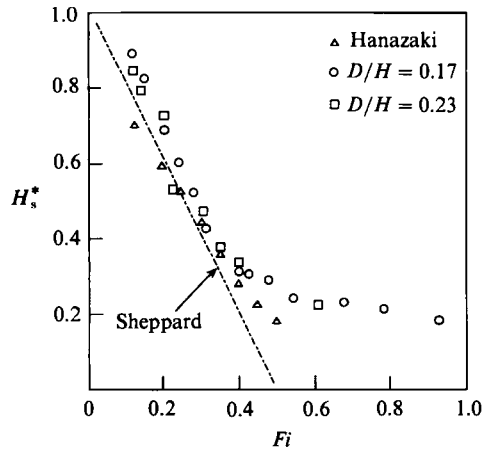


FIGURE 30. Normalized dividing streamline height against Fi .

As one notes from the shadowgraphs, fine-scale turbulence permeates the wake. For the lowest Fi experiments in this regime, the vertical scale of the turbulent wake is suppressed by stratification in the immediate lee of the sphere. For higher Fi (see figure 29c), the wake grows initially and then collapses in a manner similar to that reported by Lin & Pao (1979). Figure 29(a) demonstrates the horizontal growth of the wake owing to horizontal entrainment, and wake collapse due to stratification effects. Note that the horizontal shadowgraph is not as sharp, especially near the wake boundary, as its vertical counterpart. This is due to the fact that the second derivative of the density is much stronger in the vertical direction near the wake boundary compared to the horizontal direction.

3.9. The dividing streamline height

In the past, a number of experimental studies were done to verify Sheppard's formula (1.2). In order to determine the limits of applicability of (1.2), a series of experiments using the particle-streak technique was conducted as part of the present study. The particle-streak photographs were taken at the vertical centreplane with a relatively long time exposure to make the dividing streamline readily measurable. The results for H_s^* are plotted against Fi on figure 30, together with the calculated results of Hanazaki (1988). The agreement with Sheppard's formula is good for $Fi \lesssim 0.4$. The slope of the data indicates that $\alpha \approx 1$ in Drazin's formula (1.1).

3.10. General separation angle behaviour

One parameter that could be observed over the entire experimental Fi, Re parameter space was the horizontal separation angle, θ_H . By itself, this parameter does not reveal much information on the physical processes involved in these flows. However, a direct comparison of θ_H with the flow regime map of figure 2 may be made, and is shown in figure 31. The correspondence between the regime boundaries and the contour lines of constant angle is generally quite good. The independence of θ_H on Fi for the steady and unsteady two-dimensional attached vortices regimes is apparent in figure 31. For the lee-wave instability regime the separation angle is noted to be approximately independent of Re . The more limited vertical separation angle (θ_V) data is shown in figure 32, where the axes are identical to figure 31. The narrow vertical extent of the wake, when compared to θ_H , is apparent throughout the observed parameter ranges.

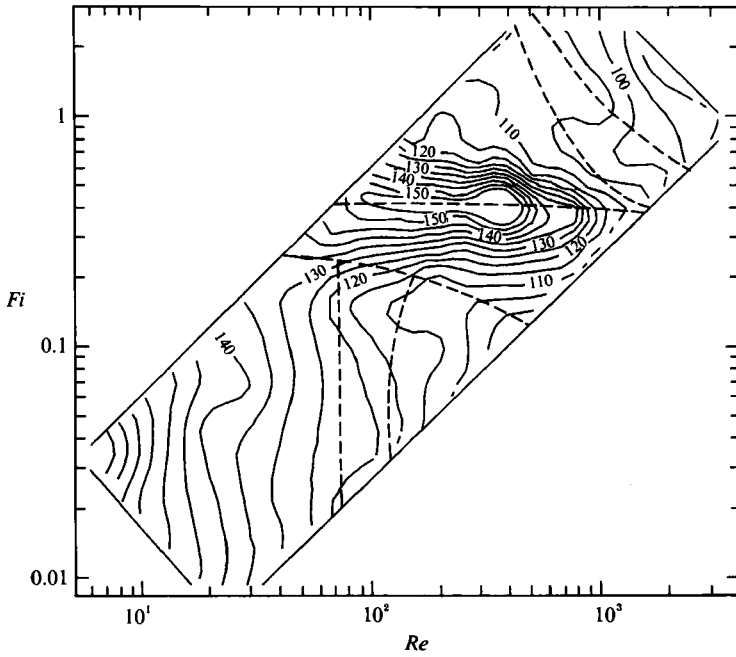


FIGURE 31. Horizontal separation angle, θ_H , as a function of Fi and Re , as shown by a contour map; the regime diagram of figure 2 is superimposed.

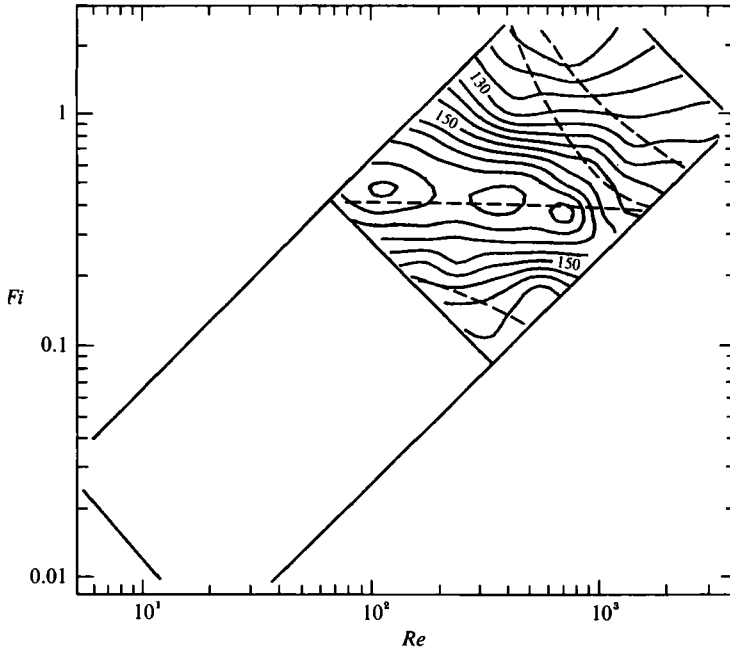


FIGURE 32. Vertical separation angle, θ_v , as a function of Fi and Re , as shown by a contour map; the regime diagram of figure 2 is superimposed.

4. Concluding remarks

Experiments on linearly stratified flow past a sphere have been conducted for the parameter ranges given by $0.005 \leq Fi \leq 15$, $5 < Re < 10000$. Eight distinct flow patterns have been described, and these regimes have been located on an Fi, Re

regime diagram. Descriptions and physical interpretations of each flow have been given. Where possible, comparisons with other reported observations are made. Specific conclusions include:

- (i) Fully attached, unseparated flows were not observed, down to $Re \approx 6$.
- (ii) For $Fi \lesssim 0.2$, the flow is constrained to horizontal planes, with strong vertical coherence and vortical wake structure, the horizontal centreline structure of which resembles homogeneous flow past long cylinders.
- (iii) When the internal wave structure is near its resonance (relative to the size of the sphere), overturning rotors are observed for $Fi \approx 0.2-0.4$. The resonant wave structure has been observed to effectively suppress separation on the sphere at the larger values of Fi .
- (iv) Flows with $Fi \approx 0.4$ represent the transition from flows which are dominated by internal wave motion to flows where wave motion, stratification and viscous effects are all equally important. Kinematic and topological arguments are used to explain this transition process.
- (v) Further increases in $Fi-Re$ yield wake flows which become increasingly unsteady, first in a very ordered, symmetric way and subsequently in a less symmetric and periodic way, until the wake flow undergoes a transition to turbulence at $Re \approx 2000$, for sufficiently large Fi .
- (vi) Owing to the inhibition of vertical modes, wakes in stratified flows have substantially larger horizontal scales than vertical ones.

Comparisons with the numerical model of Hanazaki (1988) indicate that many features of the flow are well reproduced by his calculations (e.g. no upstream blocking, wave structure, and general steady flow behaviour). Other features such as flow unsteadiness, overturning (rotors) and non-axisymmetric vortical structures are not predicted.

Several quantitative measurements for the different flow regimes are also presented. For $Fi < 0.2$, the separation bubble geometry, including length and horizontal separation angle, were measured and compared to the corresponding homogeneous flows past cylinders and spheres. Strouhal numbers for the two-dimensional vortex shedding regime were found to be $St \approx 0.2$, independent of both Re and Fi . Lee wavelengths for $Fi \geq 0.1$ in the ($y = 0$)-plane were found to be slightly overpredicted by linear theory.

The structure of the three-dimensional vortices (i.e. symmetric and non-symmetric vortex shedding regimes) were examined, where the maximum vertical size of the vortices scaled with $Fi^{0.5}$ and the Strouhal number exhibited dependence on Fi as well as Re .

Sheppard's formula for the dividing streamline was confirmed to be valid up to $Fi \approx 0.4$. The effects of an axisymmetric upstream shear were shown to alter the observed wake flow behaviour, as well as to introduce upstream recirculation flow patterns (see Appendix).

This paper represents the consolidation of the results of independent laboratory experimental research programs at the University of Wyoming and Arizona State University.

W. R. L. would like to express his appreciation to Mr Will Ackerman and Mr Jeff Rogers for their assistance in conducting the laboratory experiments at the University of Wyoming and to Mr Matthew Feeney for translating the papers by Chashechkin (1989) and Sysoeva and Chashechkin (1988).

The Arizona State University authors acknowledge, with thanks, the support of the Office of Naval Research under Grant no. N00014-90-J-4063. Thanks also goes to Dr X. Zhang for his generous help in the early period of the experiments, and to Mr Leonard Montenegro for developing the tow-tank and associated experimental systems.

Appendix. Discussion of towing methods

The use of a tow-tank for studying flow past objects in a stratified fluid has a number of advantages and some disadvantages (Gad-el-Hak 1987). The obvious advantages include being able to maintain and control the density structure and the object's velocity-time history and the capability to achieve a wide range of speeds between tests over a relatively short time. The disadvantages include the influence of the confining walls on the internal wave field and velocity structure and the finite time available for performing quantitative measurements.

For axisymmetric bodies, the method of towing is also of concern, as any attachment, will, to some degree, influence the flow. Three methods of towing have been used in these studies: a tow-wire extending through the tank centre and an aft-mounted sting (UW studies) and a tow-wire attached to an oblique angle to the tank centreline (ASU investigations). A fourth method, used by Lofquist & Purtell (1984), employed a vertical wire attached to the sphere. The upper support of the wire was towed along a horizontal track above the water surface. (This method was used to estimate drag on the sphere by measuring the angle off the vertical of the wire.) A variation of this has been used by Mason (1977) where the sphere was suspended from a long vertical wire and was allowed to traverse the tank, acting as a pendulum bob.

The along-tank tow-wire arrangement did not require an external tow carriage, allowed for tests to be easily made in both directions and did not introduce the potential of flow disturbances from a vertical traverser support. The singular disadvantage is the viscous boundary layer created by the moving wire itself. The effect of this induced boundary layer caused sufficient concern for this tow-wire arrangement to be discarded in favour of the sting mount in the UW experiments.

The induced viscous flow which exists adjacent to a tow-wire may be examined by using the solution of the suddenly accelerated infinite cylinder (Carslaw & Jaeger 1959, pp. 334-6). The viscous boundary layer behaviour, for the experimental parameters applicable to the present experiments, is shown in the dimensional plot of figure 33, where the boundary-layer thickness is shown as a function of time. An arbitrary value of $u(\delta)/U = 0.05$ (relative to a stationary observer, where $u(r)$ is the velocity in the wire-induced boundary layer) was assigned to provide an estimate of the boundary-layer thickness, $\delta_{0.05}$. The essential conclusion is that towing wires induce a strong upstream axisymmetric shear in all cases where an established flow around the sphere could be assumed. For example, if an arbitrary traverse length of ten diameters was taken to be necessary for an established flow to exist, the minimum elapsed time for any test using the present experimental parameters, would be 2.5 s at a traverse speed, $U = 5 \text{ cm s}^{-1}$ and a sphere diameter, $d = 1.27 \text{ cm}$. Another criterion for established flow would be $Nt > 1$, which, for $N \sim 1.2 \text{ s}^{-1}$, would also imply $t > 1 \text{ s}$. From figure 33, the wire-induced boundary-layer thickness for this example is $\delta_{0.05} \approx 0.4 \text{ cm}$ which is 63% of the sphere radius. All other experimental conditions developed even thicker wire-induced boundary layers.

A series of tests performed using a horizontal tow-wire provided an opportunity to examine the wake characteristics of a sphere exposed to an axisymmetric upstream

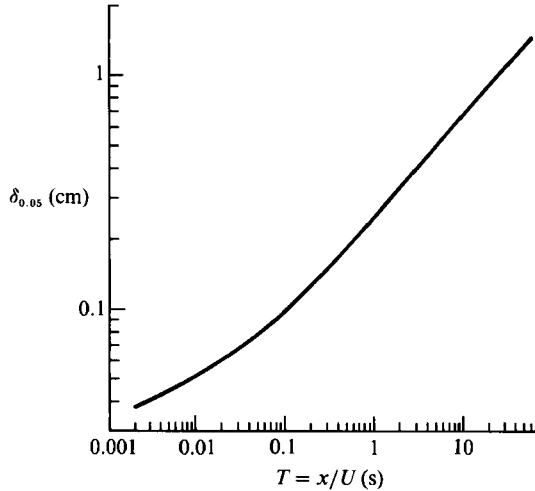


FIGURE 33. Dimensional example of the viscous boundary-layer thickness adjacent to a suddenly accelerated wire of radius r_0 , where T is the elapsed time from the initial, impulsive acceleration, in seconds. For this example, $\nu = 0.01 \text{ cm}^2 \text{ s}^{-1}$, $d = 0.05 \text{ cm}$ (the wire diameter).

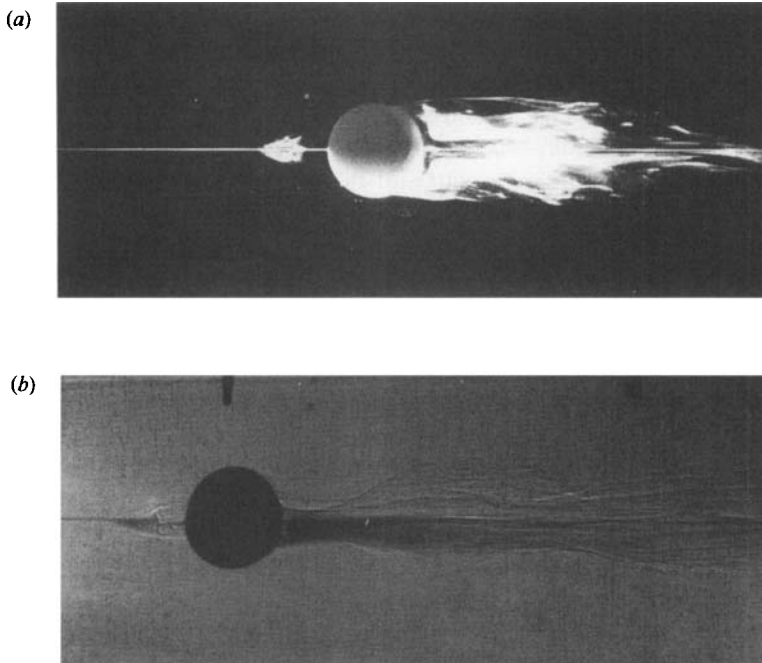


FIGURE 34. Example of upstream flow due to tow-wire induced viscous boundary layer ($Re = 1370$, $Fi = 0.38$). (a) Top view photograph, using reflective flakes; (b) side-view shadowgraph.

shear flow. A flow regime diagram was developed for the tow-wire experiments (based on over 150 tests). A comparison of the two flow regimes using the tow-wire and sting mount revealed that for the tow-wire tests:

- (i) the a_U, A_U regime extended down to $Re \approx 25$ (see figures 2 and 6);
- (ii) the v_t, V_t regime was observed down to $Re \approx 100$;

- (iii) the ℓ, L regime was observed for the same range of Fi as for the sting – the internal flow structure in the ($z = 0$)-plane within the wakes, however, correspond to the Re regime boundaries discussed above;
- (iv) n, N flows, where the two wakes were clearly separated, were not observed; and
- (v) the transition to a collapsed narrow turbulent wake occurred at lower Fi, Re values.

In summary, flow-field comparisons were not consistent between the two methods (with the exception of $Fi \approx 0.4$, for which wave motion dominates the dynamics). It is concluded that whenever viscous effects play a principal role in the near-wake structure, the along-tank tow-wire boundary layer alters the flow.

For the higher Fi tow-wire studies, the wire boundary layer created an interesting recirculation zone immediately upstream of the sphere, as shown in figure 34. These upstream recirculating zones are also visible in the photographs of Pao (1968) (as reproduced by Turner 1973) and Hopfinger (1987), and have been incorrectly termed blocking regions by Chashechkin (1989). The oblique tow-wire arrangement used in the ASU experiments eliminated the difficulties introduced by the along-tank tow-wire method.

REFERENCES

- ACHENBACH, E. 1972 Experiments on the flow past spheres at a very high Reynolds numbers. *J. Fluid Mech.* **54**, 565–575.
- ACHENBACH, E. 1974 Vortex shedding from spheres. *J. Fluid Mech.* **62**, 209–221.
- BATCHELOR, G. K. 1967 *An Introduction to Fluid Dynamics*. Cambridge University Press.
- BERGER, E. & WILLE, R. 1972 Periodic flow phenomena. *Ann. Rev. Fluid Mech.* **4**, 313–340.
- BOYER, D. L. 1968 Flow past a right circular cylinder in a rotating frame. *J. Basic Engng* **92**, 430–436.
- BOYER, D. L., DAVIES, P. A., FERNANDO, H. J. S. & ZHANG, X. 1989 Linearly stratified flow past a horizontal circular cylinder. *Phil. Trans. R. Soc. Lond.* A **328**, 501–528.
- BRIGHTON, P. W. M. 1978 Strongly stratified flow past three dimensional obstacles. *Q. J. R. Met. Soc.* **104**, 289–307.
- CARSLAW, H. S. & JAEGER, J. C. 1959 *Conduction of Heat in Solids*, 2nd edn. Oxford University Press.
- CASTRO, I. P., SNYDER, W. H. & BAINES, P. G. 1990 Obstacle drag in stratified flow. *Proc. R. Soc. Lond.* A **429**, 119–140.
- CASTRO, I. P., SNYDER, W. H. & MARSH, G. L. 1983 Stratified flow over three-dimensional ridges. *J. Fluid Mech.* **135**, 261–282.
- CHASHECHKIN, Y. D. 1989 The hydrodynamics of a sphere in a stratified liquid. *Isv. Akad. Nauk SSSR Mekh. Zhid. i Gaza*, No. 1, 3–9.
- CHASHECHKIN, Y. D. & SYSOEVA, E. I. 1988 Fine structure and symmetry of the wake past a sphere in a stratified liquid. *Proc. Sci. and Methodol. Seminar on Ship Hydrodyn.*, vol. 1, 17th session, Bulgarian Ship Hydrodynamics Centre, **10**, 1.
- CHOMAZ, J. M., BONNETON, P., BUTET, A. & PERRIER, M. 1990 Froude 4 transition in the wake of a sphere in a stratified fluid. *Bull. Am. Phys. Soc.* **35**, 2338.
- CHURCHILL, S. W. 1988 *Viscous Flows, the Practical Use of Theory*. Stoneham, MA: Butterworths.
- CRAPPER, G. D. 1959 A three-dimensional solution for waves in the lee of mountains. *J. Fluid Mech.* **6**, 51–76.
- DEBLER, W. 1973 The towing of bodies in a stratified fluid. *Intl Symp. on Stratified Flows, Novosibirsk, 1972*, ASCE, pp. 194–220.
- DEBLER, W. & FITZGERALD, P. 1971 Shadowgraphic observations of the flow past a sphere and a vertical cylinder in a density stratified liquid. *Tech. Rep. EM-71-3*, Dept of Mech. Engng, University of Michigan.

- DRAZIN, P. G. 1961 On the steady flow of a fluid of variable density over an obstacle. *Tellus* **8**, 239–251.
- GAD-EL-HAK, M. 1987 The water towing tank as an experimental facility. *Exps Fluids* **5**, 289–297.
- HANAZAKI, H. 1988 A numerical study of three-dimensional stratified flow past a sphere. *J. Fluid Mech.* **192**, 393–419.
- HONJI, H. 1987 Near wakes of a sphere in stratified fluid. *Fluid Dyn. Res.* **2**, 75–76.
- HOPFINGER, E. J. 1987 Turbulence in stratified fluids: a review. *J. Geophys. Res.* **92** (C5), 5287–5303.
- HUNT, J. C. R., ABELL, C. J., PETERKA, J. A. & WOO, H. 1978 Kinematical studies of the flows around free or surface-mounted obstacles; applying topology to flow visualization. *J. Fluid Mech.* **86**, 179–200.
- HUNT, J. C. R. & SNYDER, W. H. 1980 Experiments on stably and neutrally stratified flow over a model three-dimensional hill. *J. Fluid Mech.* **96**, 671–704.
- KIM, H. J. & DURBIN, P. A. 1988 Observations of the frequency in a sphere wake and of drag increase by acoustic excitation. *Phys. Fluids* **31**, 3260–3265.
- LIGHTHILL, M. J. 1963 In *Laminar Boundary Layers* (ed. L. Rosenhead), pp. 48–88. Oxford University Press.
- LIN, J. T. & PAO, Y. H. 1979 Wakes in stratified fluids: a review. *Ann. Rev. Fluid Mech.* **11**, 317–338.
- LOFQUIST, K. & PURTELL, P. 1984 Drag on a sphere moving horizontally through a stratified liquid. *J. Fluid Mech.* **148**, 271–284.
- MAGARVEY, R. H. & MACLATCHY, C. S. 1965 Vortices in sphere wakes. *Can. J. Phys.* **43**, 1649–1656.
- MASON, P. J. 1977 Forces on spheres moving horizontally in a rotating stratified fluid. *Geophys. Astrophys. Fluid Dyn.* **8**, 137–154.
- NAKAMURA, I. 1976 Steady wake behind a sphere. *Phys. Fluids* **19**, 5–8.
- OSTER, G. 1965 Density gradients. *Sci. Am.* **213**, 70–76.
- PAO, H. P. & KAO, T. W. 1977 Vortex structure in the wake of a sphere. *Phys. Fluids* **20**, 187–191.
- ROSENHEAD, L. 1953 Vortex systems in wakes. *Adv. Appl. Mech.* **3**, 185–195.
- ROSHKO, A. 1953 On the development of turbulent wakes from vortex streets. *NACA Tech. Note* 2913.
- SHEPPARD, P. A. 1956 Air flow over mountains. *Q. J. R. Met. Soc.* **82**, 528–529.
- SNYDER, W. H., THOMPSON, R. S., ESKRIDGE, R. E., LAWSON, R. E., CASTRO, I. P., LEE, J. T., HUNT, J. C. R. & OGAWA, Y. 1985 The structure of strongly stratified flow over hills: dividing-streamline concept. *J. Fluid Mech.* **152**, 249–288.
- SYSOEVA, H. J. & CHASHECHKIN, Y. D. 1988 The spatial structure of the path behind a sphere in a stratified liquid. *Z. Prik. Mekh. i Tekh. Fiz.* **5**, 59–65.
- TANEDA, S. 1956 Experimental investigation of the wake behind a sphere at low Reynolds numbers. *J. Phys. Soc. Japan* **11**, 1104–1108.
- TANEDA, S. 1978 Visual observations of the flow past a sphere at Reynolds numbers between 10^4 and 10^6 . *J. Fluid Mech.* **85**, 187–192.
- TOROBIN, L. B. & GAUVIN, W. H. 1959 Fundamental aspects of solids–gas flow. Part I: Introductory concepts and idealized sphere motion in viscous regime. *Can. J. Chem. Engng* **37**, 129–141.
- TOROBIN, L. B. & GAUVIN, W. H. 1959 Fundamental aspects of solids–gas flow. Part II: The sphere wake in steady laminar fluids. *Can. J. Chem. Engng* **37**, 167–176.
- TOROBIN, L. B. & GAUVIN, W. H. 1959 Fundamental aspects of solids–gas flow. Part III: Accelerated motion of a particle in a fluid. *Can. J. Chem. Engng* **37**, 224–236.
- TOROBIN, L. B. & GAUVIN, W. H. 1960 Fundamental aspects of solids–gas flow. Part IV: The effects of particle rotation, roughness and shape. *Can. J. Chem. Engng* **38**, 142–153.
- TOROBIN, L. B. & GAUVIN, W. H. 1960 Fundamental aspects of solids–gas flow. Part V: The effects of fluid turbulence on the particle drag coefficient. *Can. J. Chem. Engng* **38**, 189–200.
- TURNER, J. S. 1973 *Buoyancy Effects in Fluids*. Cambridge University Press.